

**STRUCTURAL HEALTH MONITORING
OF THE INDIAN RIVER INLET BRIDGE**

by

Jack Cardinal

A thesis submitted to the Faculty of the University of Delaware in partial fulfillment of the requirements for the degree of Honors Bachelor of Civil Engineering with Distinction.

Spring 2014

© 2014 Cardinal
All Rights Reserved

**STRUCTURAL HEALTH MONITORING
OF THE INDIAN RIVER INLET BRIDGE**

by

Jack Cardinal

Approved: _____
Michael J. Chajes, Ph.D.
Professor in charge of thesis on behalf of the Advisory Committee

Approved: _____
Harry W. Shenton, III, Ph.D.
Committee member from the Department of Civil and Environmental
Engineering

Approved: _____
Kalmia E. Kniel-Tolbert, Ph.D.
Committee member from the Board of Senior Thesis Readers

Approved: _____
Michael Arnold, Ph.D.
Director, University Honors Program

ACKNOWLEDGMENTS

First I have to thank Michael Chajes. Dr. Chajes gave me the opportunity to work on this innovative system, gain invaluable experience in structural engineering, and guided me the entire way through my undergraduate research experience. Next is Harry Shenton who acted as another mentor in an advisory role on my research. Gary Wenczel deserves special thanks for overseeing the installation of the system and being a great source for information and data, as does Nakul Ramanna who was always willing to help me in any way as I completed my work. My fellow students Hadi Al-Khateeb and Pablo Marquez were always there to advise me and collaborate with. Jack Puleo additionally gave me great guidance with his programming course and advice. Lastly, I would like to thank my family for always being there to support me in my endeavors, no matter what they are.

TABLE OF CONTENTS

| | |
|--|-----|
| TABLE OF CONTENTS | iv |
| LIST OF TABLES | vi |
| LIST OF FIGURES..... | vii |
| ABSTRACT..... | x |
| 1 INTRODUCTION | 1 |
| 1.1 Thesis Objective | 1 |
| 1.2 History of Structural Health Monitoring (SHM)..... | 1 |
| 1.3 History of Indian River Inlet Bridge (IRIB)..... | 5 |
| 1.4 Outline of Thesis..... | 9 |
| 2 DESCRIPTION OF BRIDGE | 10 |
| 2.1 Indian River Inlet Bridge..... | 10 |
| 2.2 Structural Health Monitoring System | 10 |
| 3 BRIDGE TESTS | 16 |
| 3.1 Overview of Tests | 16 |
| 3.2 Test Descriptions | 17 |
| 3.2.1 Test 1 | 17 |
| 3.2.2 Test 2 | 24 |
| 4 TEST RESULTS | 38 |
| 4.1 Analysis Method..... | 38 |
| 4.2 Sample Results From Test 1 | 40 |
| 4.2.1 Sensor Details..... | 40 |
| 4.2.2 Pass 4a's Use..... | 41 |
| 4.2.3 Peak Strains..... | 42 |
| 4.2.4 West to East Comparison..... | 43 |
| 4.2.5 Pylon Phenomenon..... | 44 |
| 4.2.6 Most Extreme Loading Conditions | 51 |
| 4.2.7 Strain in Pylons | 52 |
| 4.2.8 Fundamental Frequency..... | 53 |
| 4.2.9 Transverse Load Distribution..... | 56 |
| 4.2.10 Distribution Factors..... | 57 |

| | | |
|-------|--|----|
| 4.3 | Comparison of Two Tests | 59 |
| 4.3.1 | Compare Peak Response..... | 59 |
| 4.3.2 | Compare Similar Passes | 61 |
| 4.3.3 | Compare Load Distribution | 64 |
| 4.3.4 | Variability Discussion | 68 |
| 5 | AMBIENT RESPONSE VERSUS LOAD TESTS..... | 70 |
| 5.1 | Temperature Induced Response..... | 70 |
| 5.1.1 | Time History Investigated | 70 |
| 5.1.2 | Linear Regression..... | 72 |
| 5.1.3 | Strain Curve Fitting | 74 |
| 5.1.4 | Non Linear Regression | 75 |
| 5.1.5 | Discussion and Conclusions | 77 |
| 5.2 | Permit Vehicles..... | 78 |
| 5.2.1 | Correlation of Strain to Truck Weight..... | 78 |
| 5.2.2 | Permit Peak Load Comparison..... | 79 |
| 5.2.3 | Transverse Load Distribution to Find Permit Vehicle Positioning | 82 |
| 5.2.4 | Two Truck Train Comparison and Weight Prediction | 83 |
| 6 | FUTURE APPLICATIONS..... | 88 |
| 6.1 | Standard Test and Procedure Implementation..... | 88 |
| 6.2 | Parameters to Observe..... | 89 |
| 6.3 | Long Term Use | 89 |
| 7 | CONCLUSION | 91 |
| | REFERENCES | 92 |
| A | MATLAB CODE | 94 |
| A.1 | Linear Regression | 94 |
| A.2 | Strain Fitting | 96 |
| A.3 | Nonlinear Fitting..... | 97 |

LIST OF TABLES

| | | |
|----------|--|----|
| Table 1 | Distribution Factors for One Truck Per Lane | 58 |
| Table 2 | Distribution Factors for a Two Truck Train Per Lane | 58 |
| Table 3 | Distribution Factors for a Four Truck Per Lane | 59 |
| Table 4 | Percent Difference in Response from April to November Load Test..... | 61 |
| Table 5 | Truck Weight Comparison by Test..... | 69 |
| Table 7 | Weight by Axle and Resulting Strains for Permit Vehicles..... | 80 |
| Table 8 | Wheel Spacing of Permit Vehicles | 80 |
| Table 9 | Approximation of Permit Vehicle Weight Based on Equation (3)..... | 81 |
| Table 10 | Probable Locations of Permit Vehicles..... | 83 |
| Table 11 | Final Estimated Permit Vehicle Gross Weight..... | 87 |

LIST OF FIGURES

| | | |
|-----------|---|----|
| Figure 1 | Location Map of the Indian River Inlet Bridge | 6 |
| Figure 2 | Elevation View of the Indian River Inlet Bridge..... | 8 |
| Figure 3 | Uniaxial and Biaxial Accelerometer Locations..... | 13 |
| Figure 4 | Sensor Zone Locations and Labeling..... | 14 |
| Figure 5 | Test 1 Truck Numbers with Axle Weights and Spacings | 19 |
| Figure 6 | Test 1 Single Truck Pass Diagrams | 21 |
| Figure 7 | Test 1 Double Truck Pass Diagrams..... | 22 |
| Figure 8 | Test 2 Four Truck Pass Diagrams..... | 23 |
| Figure 9 | Test 1 Dynamic Truck Pass Diagrams | 24 |
| Figure 10 | Test 2 Truck Numbers with Axle Weights and Spacings | 25 |
| Figure 11 | Test 2 Truck Numbers with Axle Weights and Spacings Continued | 26 |
| Figure 12 | Test 2 Pass Diagrams, Stages 1 to 3 | 29 |
| Figure 13 | Test 2 Pass Diagrams, Stages 4 and 5 | 30 |
| Figure 14 | Test 2 Pass Diagrams, Stages 6 and 7 | 31 |
| Figure 15 | Test 2 Pass Diagrams, Stages 8 and 9 | 32 |
| Figure 16 | Test 2 Pass Diagrams, Stages 10 and 11 | 33 |
| Figure 17 | Test 2 Pass Diagrams, Stages 12 and 13 | 34 |
| Figure 18 | Test 2 Pass Diagrams, Stages 14 and 15, Dynamic Passes | 36 |
| Figure 19 | Test 2 Pass Diagrams, Stage 16, Transverse Placement | 37 |
| Figure 20 | Deck Cross Section | 44 |

| | | |
|-----------|---|----|
| Figure 21 | Mislabeling of Strain Sensor S_W29E (Seconds vs. Microstrain) | 45 |
| Figure 22 | Floating Sensor S_E23N (Seconds vs. Microstrain) | 46 |
| Figure 23 | Floating Sensor S_W23N (Seconds vs. Microstrain) | 46 |
| Figure 24 | Bottom Array Pylon Strain (Seconds vs. Microstrain) | 47 |
| Figure 25 | Top Array Pylon Strain (Seconds vs. Microstrain)..... | 48 |
| Figure 26 | Truck Movement Across Bridge | 49 |
| Figure 27 | Top Array Strain, Northwestern Pylon (Seconds vs. Microstrain)..... | 50 |
| Figure 28 | Pylon Cross Section Underneath Deck | 53 |
| Figure 29 | S_W8 Initial Data from 105 Seconds to End of Time Series | 55 |
| Figure 30 | S_W8 Demeaned Data from 105 Seconds to End of Time Series | 55 |
| Figure 31 | S_W8 Fundamental Frequency | 56 |
| Figure 32 | Percentages of Loading Using S_W8, Truck Moving Transversely West to East..... | 57 |
| Figure 33 | April vs. November Pass 4a Comparison..... | 62 |
| Figure 34 | April Pass 6a Compared to November Pass 4a | 63 |
| Figure 35 | Test 2 Transverse Load Distribution at S_W8 | 65 |
| Figure 36 | Transverse Load Distribution at S_W8 of Test 1 (Red) Compared to Test 2 (Blue) | 66 |
| Figure 37 | Test 2 Transverse Load Distribution from S_W6..... | 67 |
| Figure 38 | Test 2 Transverse Load Distribution from S_W2..... | 68 |
| Figure 39 | 10 Day Time History of Strain in S_W8 and Relative Temperature | 71 |
| Figure 40 | Temperature (Fahrenheit) versus Microstrain for Sensor S_W8..... | 72 |
| Figure 41 | Linear Model for Microstrain as a Result of Temperature..... | 73 |
| Figure 42 | Strain Model (5) and S_W8 Over 10 Day Span | 75 |

| | | |
|-----------|--|----|
| Figure 43 | Power Model for Microstrain as a Result of Temperature..... | 76 |
| Figure 44 | Permit Vehicle Wheel Spacing Diagram | 80 |
| Figure 45 | September 6 th , 2013 Permit Vehicle Strain Time History..... | 84 |
| Figure 46 | April Load Test, Pass 2b, Location SW_22 | 85 |

ABSTRACT

The Indian River Inlet Bridge, located in Sussex County, Delaware, is a critical portion of the Route 1 Coastal Highway and allows many beach goers access to the Delaware shores. This concrete, cable stayed bridge was completed in early 2012 and just recently opened to full capacity. A Structural Health Monitoring (SHM) system was designed and installed into the bridge during the construction process and on April 30th the University of Delaware conducted a calibration load test. The data was then analyzed and evaluated to determine the nominal response of the bridge based upon the collected data. Using smoothing techniques, the immense amount of data was processed and different aspects of the bridge were investigated. This was then put into a load test report for the Delaware Department of Transportation (DelDOT). By primarily using strain data many areas were investigated. The fundamental period of the bridge was determined along with the maximum loading conditions that the bridge underwent. Distribution factors were calculated using a transverse flow of load analysis and many other responses that the bridge experienced during loading were delved into. These topics and more were all combined for a comprehensive overview of the bridge's performance.

A second load test on November 28, 2012 was conducted to induce different responses in the bridge with varying formations and to test the repeatability of the data recorded during the April test. The comparison between the tests was done by examining each test's truck weights, peak responses, load distributions and time

history responses. As a result of conducting this comparison the system's overall accuracy was evaluated.

Lastly, with this work there are many future applications that this system can be used for. Examples of such future uses would be the creation of standard testing procedure for the Indian River Inlet Bridge, extreme load monitoring, determining a loading threshold, as well as what ambient response data looks like on the bridge. As a result of examining permit loads a method was determined to predict vehicle weights on the bridge and an investigation into temperatures effects on strain gauges was completed. Overall, the Indian River Inlet Bridge's integrated structural health monitoring system gives a high quality picture of the "health" of the bridge and has future applications in both monitoring and research.

Chapter 1

INTRODUCTION

1.1 Thesis Objective

The objective of this thesis was to first determine the baseline response of the Indian River Inlet Bridge and its structural health monitoring system through large scale load testing. Secondly, by conducting a second load test the goal was then to determine how repeatable the response of the bridge was. This work culminates in the creation of a load test report presented to DelDOT, but here goes into much more detail. Overall, the goal was to compile the entirety of my work on the Indian River Inlet Bridge into one document.

1.2 History of Structural Health Monitoring (SHM)

After a catastrophic failure of a manmade object, which could have resulted in injury or the loss of life, a team of investigators comes to inspect the site to determine exactly went wrong and why. There could possibly be a more efficient and safer way to avoid these types of situations however, and that is by employing the idea of structural health monitoring systems. Structural health monitoring (SHM) is the process by which a material or structure can record readings about its physical state and condition over time, making them readily available to a user. This is achieved through the use of a multitude of integrated sensors that can differ drastically in function, but mesh together to give an overall picture of the structure or material's status. There are many motivations for the use of SHM systems in civil structures.

These include increasing the knowledge regarding the safety of the structure, mitigation of catastrophic failure with huge loss of life due to constant monitoring, confirmation of assumptions made during design, allowing for the ease of pinpointing problems and their maintenance, and the economic benefits of building and repairing more efficiently (Balageas 2006). The topic of SHM is rising to the forefront of civil engineering, especially in the field of bridge building as a result of the degradation of bridges built many years ago. According to Aftab A. Mufti of the University of Manitoba and of Intelligent Sensing for Innovative Structures Canada, in the United States there are around 200,000 structurally degraded bridges and that between 150-200 bridges collapse per year (Mufti 2002). These statistics certainly spur interest in SHM systems for bridges. Over approximately the past 20 years, SHM systems have become an innovative and useful topic in bridge engineering and have been implemented throughout the world using numerous different systems and sensors.

There is no specific bridge or time that has been recorded where the first SHM system was used. To start off there were bridges that were instrumented only with minor sensors and gauges at a single point to determine the response at a certain location. As SHM systems have advanced, many different monitoring systems have been established. First, standard sensors, such as vibrating wire strain gauges and foil strain gauges, were attached to the outside of the bridge and were used to get strain readings on the bridge from applied loads in certain locations (CTL Group 2011). Other civil engineers focused on using Global Positioning Systems (GPS) to create an artificial neural network to help measure deformations of the bridge, to record real time displacements of the bridge and create a constantly updating computer model (Akyrlmaz 2004). As of late there has been more use of fiber optic cables and

fiber Bragg-Grating sensors. These sensors are advantageous because they resist noise during data collection from electronic sources that plague standard sensors and also have a decently long life in the field if handled correctly (SMARTEC 2008). A fiber Bragg-Grating sensor has a grating that reflects a spectral peak that depends on the grating spacing of the sensor. When the sensor is stretched in tension or shortened in compression, it receives a different wavelength of light reflected back that can be extrapolated to a strain or other type of reading (Schulz 2001). These fiber optic and fiber Bragg-Grating sensors are also becoming cheaper and better functioning over time (Doornick 2005). No matter what type of sensor is used, there needs to be a process of data collection by an interrogating system that is efficient, organized, and presentable so that the data can be used effectively by bridge owners. All of these varying sensing methods can be used in conjunction with one another to give the best SHM system possible for a specific bridge and for a certain purpose.

Structural health monitoring systems can be used for many different purposes based upon the bridge project, type and location. A prime reason for adopting a system is to monitor a bridge as it is being rehabilitated to ensure the safety of continued traffic and to show that the rehabilitations had the desired effect. In 2007 a renovation began on the Huey P. Long Bridge that crosses the Mississippi in Louisiana to improve traffic flow by widening the bridge as well as keeping train traffic flowing by only renovating and not replacing the bridge. The bridge was instrumented with 777 vibrating wire strain gauges that were attached to 433 members in order to monitor the bridge through the entirety of the expansion project through 2011 (CTL Group 2011). Another reason that bridge monitoring systems are used is that they can be used to monitor a bridge that is in a geographically demanding

location. Two examples of this condition are the Tsing Ma Bridge in Hong Kong and the Fatih Sultan Mehmet Bridge in Istanbul, Turkey. The Tsing Ma was outfitted due to the high wind the bridge experiences from storms (Jiang 2002) and the Fatih Sultan Mehmet is located directly in the North Anatolian Fault Zone that is known for its earthquakes (Akyilmaz 2004). Constant monitoring will keep engineers informed of the bridge's degradation over time and prevent a catastrophic failure with high casualties because of rehabilitations that will protect against the environment's affects. Lastly, there are bridges that are being built with sensors integrated into them from the start to keep track of the functioning of the bridge throughout its lifetime. After the I-35W St. Anthony Fall's collapse in Minneapolis, Minnesota during 2007, there was a push to replace the failed bridge with one that would have an integrated monitoring system. As the bridge was built, the SHM system installation was tailored to the construction schedule and was embedded into the bridge. This increased the knowledge of the safety of the bridge and gave the public the security they desired (Inaudi 2009).

The direction of the future are these integrated SHM systems that monitor a bridge's activity in real time and can be used to provide diagnostic reports when desired. These systems use wireless, smart sensors that are imbedded into the bridge during the construction phase and send data at a certain collection rate to an interrogator that acquires the data (Inaudi 2009). This makes the SHM system used unique for each individual bridge because it appeals to the bridge's and its engineer's needs. A majority of the instruments used range from accelerometers, strain gauges, to those that collect temperature, displacement, tilt, corrosion, humidity, wind speed, and any other sensor that would be beneficial for the bridge's type or environment.

There can be many issues during the installation process and after installation with sensors such as not pre-tensioning gauges, workers damaging the sensors during construction, gauges sliding making them acquire no data, and water penetration (Enckell 2007). Errors like these can be prevented in the future as workers and installers gain more experience with the systems. As technology advances most of these integrated systems are utilizing fiber optic and fiber Bragg-Grating sensors. These sensors are seen as more durable in the engineering community. The Intelligent Sensing for Innovative Structures (ISIS) Canada outfitted the Beddington Trail Bridge in Alberta, Canada with fiber optic sensors and in 1999, six years after the systems introduction, load tested the bridge and showed that every single sensor was still functioning, contributing to the notion that fiber optic sensors are durable and long lasting (Mufti 2002). These sensors need to be tough in order to have the same lifespan as the bridge they are sensing, which is on average around one hundred years. Fiber optics additionally reduces the noise on the data collected because they are immune to electrical noise interference (West 2005). A recent example of a bridge that primarily uses fiber optic and fiber Bragg-Grating sensors is the Indian River Inlet Bridge (Charles W. Cullen Bridge) located in Delaware of the United States.

1.3 History of Indian River Inlet Bridge (IRIB)

The Indian River Inlet Bridge is on State Route 1 (SR-1) Coastal Highway and is the primary way for many beach goers to reach the Delaware beaches, so the bridge undergoes a lot of traffic and is of the utmost importance to Delaware residence. The bridge spans the Indian River Inlet and connects Dewey Beach and Bethany Beach using SR-1. The inlet is not only integral in the passage of car traffic but also for

boaters traveling into and out of the Indian River Bay's marinas to the Atlantic Ocean. The location of the bridge can be seen in Figure 1.

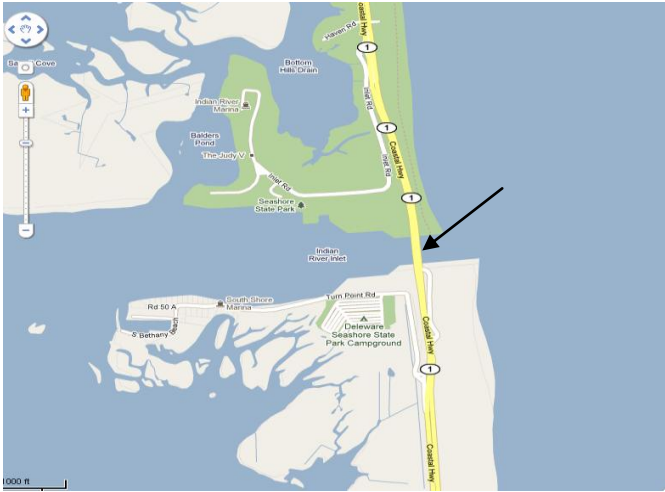


Figure 1 Location Map of the Indian River Inlet Bridge

Over the past century, there have been numerous bridges used to span the Indian River Inlet. Bridges were built in 1934, 1938, 1952, 1965, and in 2012 being the latest bridge. The first structure was constructed out of timber and was followed by two swing span bridges who's life spans were both around ten years. In 1965, twin spans were constructed with the hope that they would function for a longer period of time. The twin spans were not completed at the same time however. The structure foundations of both bridges and the northbound bridge superstructure were completed in 1965, while the southbound superstructure was finished in 1976 (Stuffle 2006). This twin span bridge had piers located in the inlet for its foundation system which created major issues with scour around the piles due to the intense tidal flow into and out of the inlet. Even with scour mitigation projects during the 80's and 90's,

the scour got so extreme that the bridge became rated structurally deficient, yet still safe for travel. It was decided by The Delaware Department of Transportation (DeIDOT) that in order to avoid the possibility of having to close the bridges entirely, decimating beach businesses, DeIDOT decided to build another bridge as they kept the twin spans open.

The main motivation of this new bridge would be to completely span the Inlet, leaving no possibility of the bridge developing scour issues in the future, as well as to leave room for future widening of the inlet if boat traffic increased. In 2004, Figg Engineering designed plans for the replacement bridge using an ornate arch design. However, this bid ended up overshooting their budgeting by 50 million dollars, making DeIDOT put the project back out to bid in 2006. By 2008 the project was won by the design firm Skanska. Skanska designed the current cable stayed bridge, using AECOM to help facilitate building the structure. As the bridge was constructed the University of Delaware partnered with the builders to outfit the bridge with an integrated structural health monitoring system. This makes the current Indian River Inlet Bridge, completed in January of 2012, one of the only bridges of its kind in North America. Figure 2 is an elevation view picture taken during the second load test.



Figure 2 Elevation View of the Indian River Inlet Bridge

The concrete, cable stayed bridge which has a main span of 900 feet and a total length of 1,750 feet was instrumented with a variety of different sensors, primarily fiber optic. The sensors for data acquisition include 70 integrated strain and temperature sensors, 27 accelerometers (Biaxial, uniaxial), 9 inclination measuring tilt meters, 3 displacement sensors, 2 anemometers, and 16 chloride sensors, totaling to 127 independent sensors collecting data on 197 variables (Shenton 2011). The SHM system was implemented on this bridge by the University of Delaware Center for Innovative Bridge Engineering (CIBrE) and the contractors of the bridge for a few different purposes. These reasons included being able to see if measured data from the system correlated well with the model created by the design team when put under the same conditions, to help the owner, DeIDOT, understand how the bridge functions throughout its lifetime, and to ease the maintenance and upkeep of the bridge. Lastly, the Indian River Inlet Bridge monitoring project, being one of the first of its kind, will

be useful as a case to be studied by other groups trying to instrument their bridges with SHM systems as well (West 2005).

1.4 Outline of Thesis

First, I will discuss the Indian River Inlet Bridge as well as the system integrated into the structure. Following that, the bridge tests will be described as well as the results acquired by the first load test. Next, a comparison of the second load test to the first is made in order to discuss variability. As a result of these load tests an interesting discussion can be made regarding ambient responses compared to responses induced due to load tests. Lastly, before concluding, the future applications of the structural health monitoring system of the Indian River Inlet Bridge are examined.

Chapter 2

DESCRIPTION OF BRIDGE

2.1 Indian River Inlet Bridge

The tested concrete cable stayed bridge, completed in early 2012, consists of a combination of pre-cast and cast in place reinforced concrete. The total length of the bridge is 1,750 feet with a main span of 900 feet and a typical width of 105 feet. There are four, 250 foot tall pylons supporting the bridge with 19 stay cables per pylon. These pylons are spaced 900 feet apart and will allow for any future widening of the 300 foot wide inlet over the duration of the bridge's lifespan.

2.2 Structural Health Monitoring System

The Indian River Inlet Bridge is outfitted with fiber-optic sensors developed by Cleveland Electric Laboratories (CEL) and Chandler Monitoring Systems (CMS) who additionally supplied two Micron Optics model SM130 interrogators for acquiring the data. The 70 strain sensors measure temperature as well as the strain in the bridge. These sensors are in 3 out of the 4 pylons and along the deck are located at the top and bottom of the edge girders. In the pylons there are four strain gauges located at the centerline of each of the 4 pylon walls, creating an array of sensors. There are two elevations of this array throughout each instrumented pylon, one lower and one higher than the other. Along the two edge girders of the bridge the strain/temperature sensors are placed in the tensile and compressive regions of the girder to attain axial forces

and bending moments. Throughout the bridge there are 17 cross sections of strain sensors on the edge girders. Additionally, there are 27 accelerometers spread out across the bridge, primarily concentrated on the eastern side. There is one biaxial accelerometer placed at the top of 3 out of 4 of the bridge pylons along with one uniaxial on top of the Northeastern pylon, 6 uniaxial and 3 biaxial accelerometers located on the East side of the deck placed at the $\frac{1}{4}$ points of each span, eight biaxial accelerometers on eight of the Northeastern pylon's stay cables, two biaxial accelerometers on the Northwestern pylon's stay cables, and one biaxial accelerometer on a Northwestern pylon stay. Additionally, there are three uniaxial accelerometers spread across the West side of the deck. Figure 3 details the approximate placement and type of accelerometers distributed across the bridge. Nine tiltmeters are distributed across the Eastern side of the deck at $\frac{1}{4}$ points and bearing supports. Coupled with these are three linear displacement sensors placed at the expansion joints of the bridge. Sixteen chloride sensors, six fiber optic and ten conventional, were spread across primarily the Eastern deck of the bridge. Lastly, two anemometers are located on the bridge, one at the peak of the North Eastern pylon and one located at deck level, mid-span of the bridge. During the test every sensor collected data besides all the chloride sensors, 2 accelerometers that were under repair, and the anemometers on the top of the pylons.

All of these sensors are depicted in Figure 2. As a result of this sketch, it can be seen that most of the strain/temperature sensors, tiltmeters, and displacement gauges are concentrated in zones 1, 2, 3 and 4, with a few accelerometers spread in. In zone 5 and 6, the strain/temperature sensor arrays are shown at their two different

heights per pylon. Lastly, in zone 7 of the sketch, all of the cable stay accelerometers can be seen.

All of the sensors were connected to two Micron Optics model SM130 interrogators and were read simultaneously. There were two different sampling rates of 125 samples/second and 250 samples/second used for the data acquisition. The sampling rate of 250 samples/second was required for the collection of data from the cable stay accelerometers, which needed a faster sampling rate to acquire precise and accurate data. The sampling rate of 125 samples/second was sufficient enough for all other sensors present during the test.

Chapter 3

BRIDGE TESTS

3.1 Overview of Tests

Load tests of the Indian River Inlet Bridge were set up to be done in April of 2012 right before the complete opening of the bridge and at six month intervals after the first one was conducted. The hope in the future is to have load tests every two years after the first year and a half of conducting 3 tests at 6 month intervals. The first load test in April of 2012 was used to help calibrate the system, confirm that the sensors were working correctly, and to give an overall picture of the performance and “health” of the newly completed bridge. The second load test detailed in this paper was to help determine the repeatability of the data when compared to the first test, give an update on the performance of the bridge, and to investigate and induce different responses in the bridge that were of interest. Overall, the final product of these load tests was to produce a load test report to be submitted to DelDOT to give a picture of how the bridge is performing. In the future, which will be discussed further on in this work, the system will be used to output load test reports created by the system itself so that DelDOT can monitor the bridge easily.

In order to minimize the impact on traffic crossing the bridge, the tests were conducted starting around 11:00 pm on low volume travel days of the week. The University of Delaware team would meet together in the staging area around 9:00 pm, get set up, explain the formations to be used and the driving expectations to the DelDOT truck drivers, and await Maintenance of Traffic’s (MOT) arrival. During this

time truck axle weights and numbers were confirmed. These trucks nominally weighed 64 kips. Once MOT arrived on scene we would conduct our passes. The bridge could only be closed with MOT keeping traffic stopped for 15 minutes at a time. After the 15 minutes passed, we would open up the flow of traffic. Most of the time, when the passes were planned well, two passes would be completed in the 15 minute time interval.

During the tests Professor Shenton would monitor and set the data logger to record. He would make sure the logger was recording as expected, saving the data after each pass. Professor Chajes and I were located on top of the deck to record truck numbers and make sure the formations were executed seamlessly. Another student normally would be located in the lead truck to help coordinate the passes. Other University of Delaware personal were located at different points on the bridge to help promote safety and accuracy. The whole test usually was completed in 3.5 to 4 hours of on bridge time.

3.2 Test Descriptions

For each one of the tests there were a different amount of passes, formations, and truck weights. The April 2012 test is labeled as Test 1 while Test 2 is the load test conducted in November 2012.

3.2.1 Test 1

Four, fully loaded 10-wheel dump trucks were used as a controlled live load for the test. The truck axles were weighed by the DeIDOT truck drivers offsite and confirmed onsite using portable truck scales. The gross weight of truck number 2829 was 63.2 kips, with a front axle weight of 15.9 kips, center axle weight of 23.8 kips,

and rear axle weight of 23.6 kips. The gross weight of truck number 2677 was 63.7 kips, with a front axle weight of 17.4 kips, center axle weight of 23.2 kips, and rear axle weight of 23.1 kips. The gross weight of truck number 2784 was 63.4 kips, with a front axle weight of 17 kips, center axle weight of 23.6 kips, and rear axle weight of 22.9 kips. Lastly, the gross weight of truck number 2904 was 63.6 kips, with a front axle weight of 17.1 kips, center axle weight of 23.3 kips, and rear axle weight of 23.2 kips. Attached sketched Figure 5 gives the wheel spacing's and wheel loads of each truck.

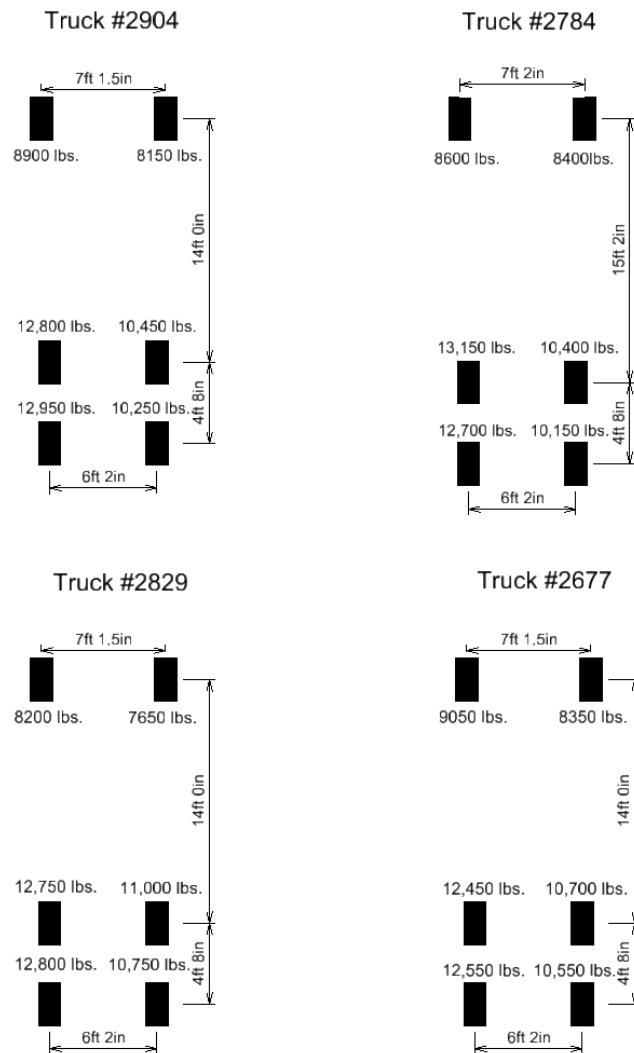


Figure 5 Test 1 Truck Numbers with Axle Weights and Spacings

Two different types of load passes (load cases) were made for the test: slow passes (approximately 10 mph) and dynamic passes (approximately 55 mph). There were 17 total load passes overall, fifteen being slow crawl passes while two were dynamic passes. The slow passes are described here. The first four passes were single truck passes by the same truck in each of the four lanes. Next, six passes were made

with two trucks in specified formations. Lastly, five passes were conducted in which all four trucks were used in different formations. The pass number and the truck formations for the slow passes:

Single Truck Passes:

Pass #1 (1a): truck on southbound slow-lane

Pass #2 (1d): truck on northbound slow-lane

Pass #3 (1b): truck on southbound fast-lane

Pass #4 (1c): truck on northbound fast-lane

Double Truck Passes:

Pass #5 (2a): both trucks southbound side by side, one fast-lane, one slow-lane

Pass #6 (2d): both trucks northbound side by side, one fast-lane, one slow-lane

Pass #7 (2b): both trucks southbound in succession, both in slow-lane

Pass #8 (2f): both trucks northbound in succession, both in slow-lane

Pass #9 (2c): both trucks southbound in succession, both in fast-lane

Pass #10 (2e): both trucks northbound in succession, both in fast-lane

Four Truck Passes:

Pass #11 (4a): all trucks traveling southbound side by side, one in each lane

Pass #12 (4c): all trucks traveling northbound in square formation

Pass #13 (4b): all trucks traveling southbound in square formation

Pass #14 (4e): all trucks traveling northbound in succession, all in slow-lane

Pass #15 (4d): all trucks traveling southbound in succession, all in slow-lane

The previously described formations are detailed in Figures 6, 7, and 8.

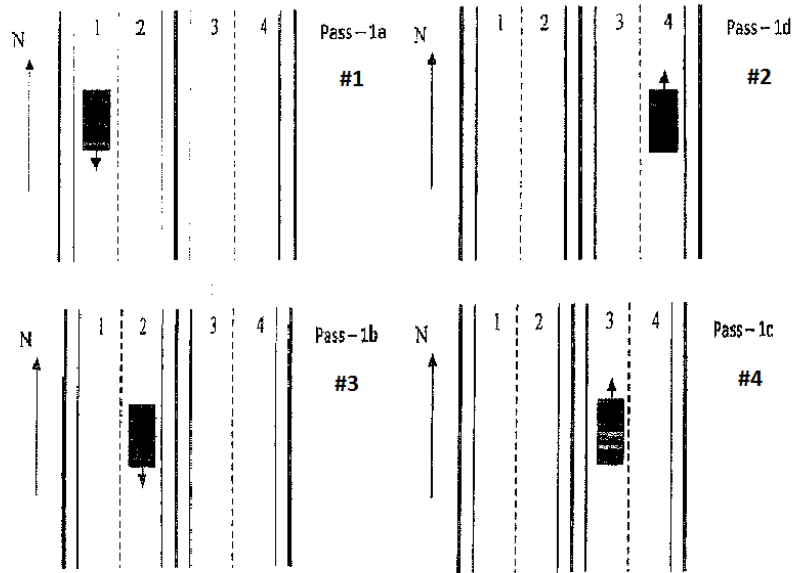


Figure 6 Test 1 Single Truck Pass Diagrams

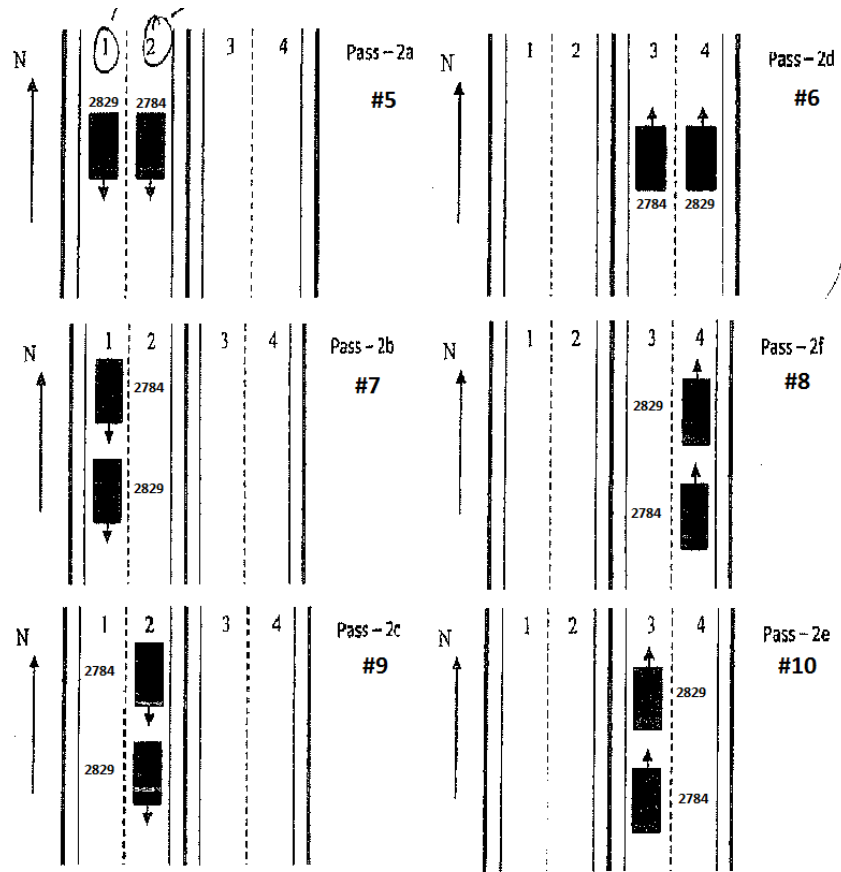


Figure 7 Test 1 Double Truck Pass Diagrams

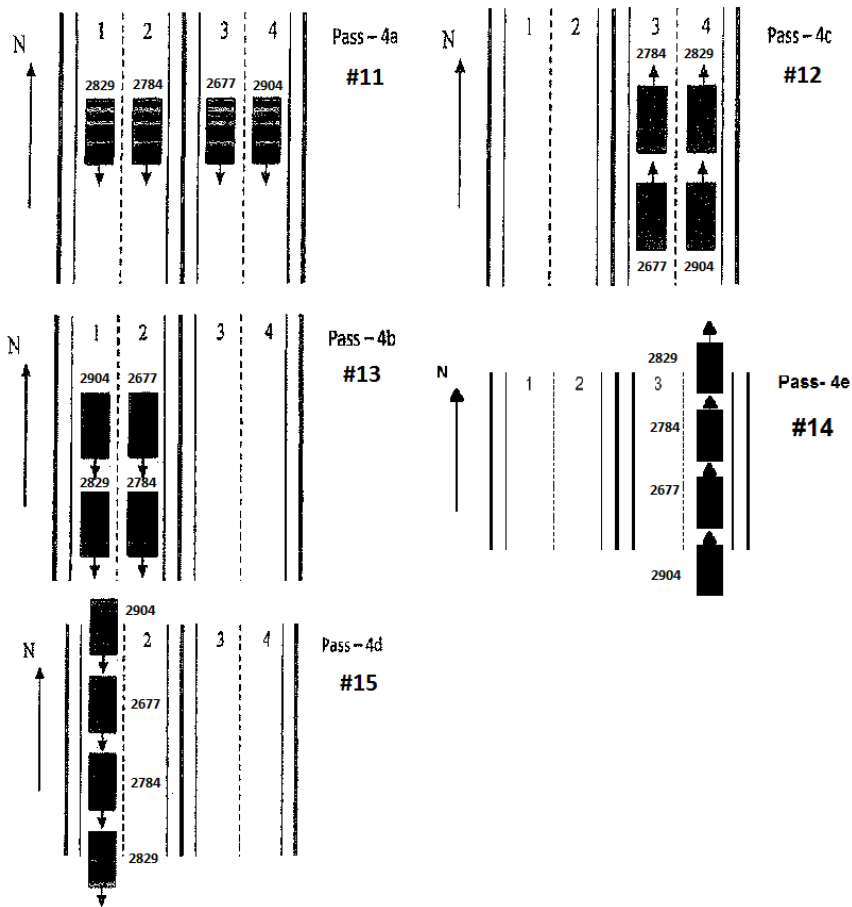


Figure 8 Test 2 Four Truck Pass Diagrams

For the dynamic passes the four vehicles traveled both southbound and northbound across the span. These dynamic tests were conducted at approximately 55 mph with 100 foot intervals between the trucks at top speed:

Dynamic Truck Passes:

Pass #16 (4f): all trucks traveling northbound in succession, all in slow-lane

Pass #17 (4g): all trucks traveling southbound in succession, all in slow-lane

The previously described formations are detailed in Figure 9.

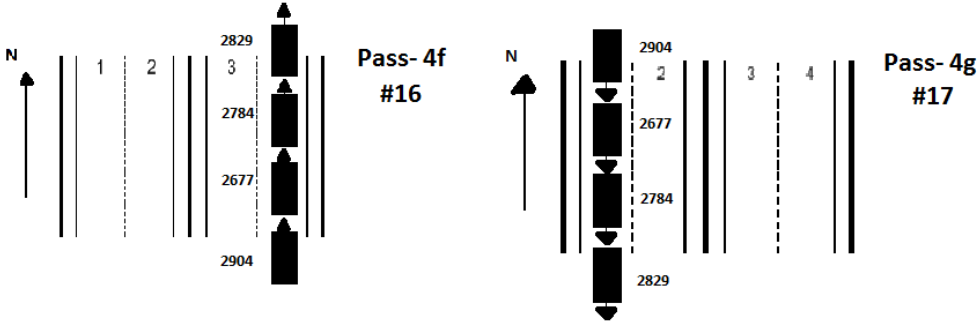


Figure 9 Test 1 Dynamic Truck Pass Diagrams

3.2.2 Test 2

Six, fully loaded 10-wheel dump trucks were used as a controlled live load for the test. The truck axles were weighed by the DeIDOT truck drivers offsite and confirmed onsite using portable truck scales. The gross weight of truck number 2969 was 62.5 kips, with a front axle weight of 15.7 kips, center axle weight of 23.4 kips, and rear axle weight of 23.4 kips. The gross weight of truck number 2829 was 63.2 kips, with a front axle weight of 15.7 kips, center axle weight of 23.7 kips, and rear axle weight of 23.9 kips. The gross weight of truck number 2784 was 62.4 kips, with a front axle weight of 15.6 kips, center axle weight of 23.5 kips, and rear axle weight of 23.3 kips. The gross weight of truck number 2758 was 61.2 kips, with a front axle weight of 16.5 kips, center axle weight of 22.6 kips, and rear axle weight of 22.2 kips.

The gross weight of truck number 2771 was 62.4 kips, with a front axle weight of 15.2 kips, center axle weight of 23.7 kips, and rear axle weight of 23.6 kips. Lastly, the gross weight of truck number 2677 was 62.7 kips, with a front axle weight of 16.1 kips, center axle weight of 23.4 kips, and rear axle weight of 23.3 kips. Attached Figure 10 and 11 give the wheel spacing's and wheel loads of each truck.

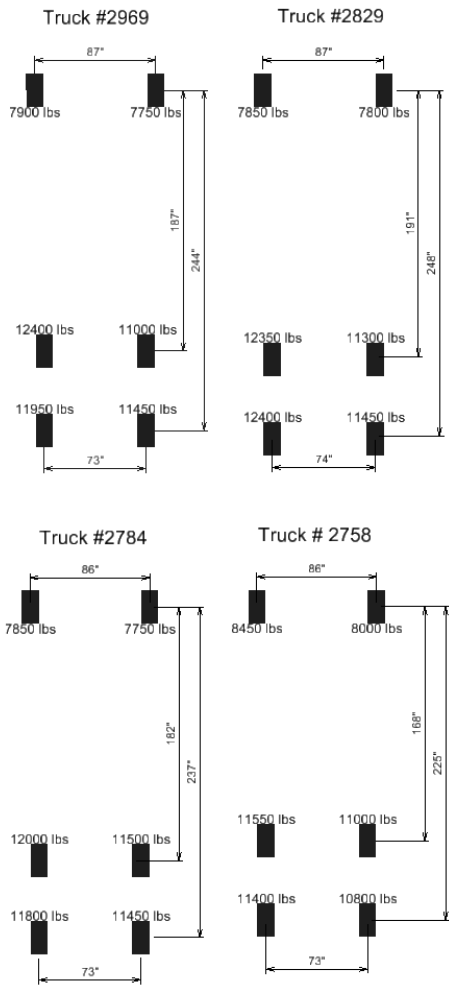


Figure 10 Test 2 Truck Numbers with Axle Weights and Spacings

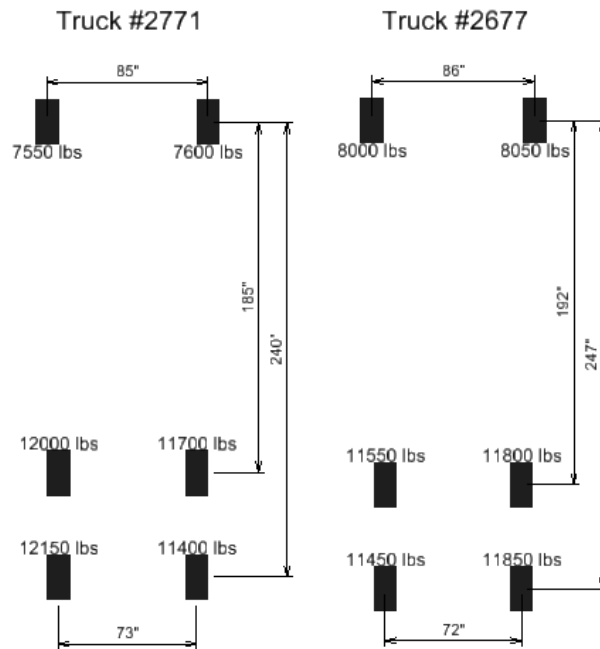


Figure 11 Test 2 Truck Numbers with Axle Weights and Spacings Continued

Two different types of load passes (load cases) were made for the test: slow passes and dynamic passes. There were 26 total load passes overall, 23 being slow crawl passes, two dynamic passes, and one being a transverse positioning of a single truck at different points on the bridge. The passes are shown in stages to illustrate the thought process and order of each pass to effectively make use of truck formations to decrease the duration of the load test. The slow passes are described here. Six passes were single truck passes by a truck in each of the four lanes and the two shoulders. Next, eight passes were made with two trucks in specified formations. Then two passes were made with three trucks side by side, one pass being on the northbound side and one pass on the southbound side. Five passes were conducted in which all

four trucks were used in different formations. Lastly, six trucks were run side by side using the four lanes and shoulders both northbound and southbound. The pass number and the truck formations for the slow passes:

Single Truck Passes:

Pass #1 (1e): truck on southbound shoulder

Pass #2 (1a): truck on southbound slow-lane

Pass #3 (1b): truck on southbound fast-lane

Pass #5 (1f): truck on northbound shoulder

Pass #6 (1d): truck on northbound slow-lane

Pass #7 (1c): truck on northbound fast-lane

Double Truck Passes:

Pass #9 (2g): both trucks southbound side by side, one slow-lane, one shoulder

Pass #10 (2a): both trucks southbound side by side, one fast-lane, one slow-lane

Pass #11 (2b): both trucks southbound in succession, both in slow-lane

Pass #12 (2h): both trucks northbound side by side, one slow-lane, one shoulder

Pass #13 (2d): both trucks northbound side by side, one fast-lane, one slow-lane

Pass #14 (2f): both trucks in northbound in succession, both in slow-lane

Pass #15 (2c): both trucks southbound in succession, both in fast-lane

Pass #17 (2e): both trucks northbound in succession, both in fast-lane

Triple Truck Passes:

Pass #4 (3a): three trucks southbound side by side, one fast-lane, one slow-lane, one shoulder

Pass #8 (3b): Three trucks northbound side by side, one fast-lane, one slow-lane, one shoulder

Four Truck Passes:

Pass #16 (4b): all trucks traveling southbound in square formation

Pass #18 (4c): all trucks traveling northbound in square formation

Pass #21 (4a): all trucks traveling southbound side by side, one in each lane

Pass #22 (4e): all trucks traveling northbound in succession, all in slow-lane

Pass #23 (4d): all trucks traveling southbound in succession, all in slow-lane

Six Truck Passes:

Pass #19 (6a): all trucks traveling southbound side by side, one in each lane including shoulders

Pass #20 (6b): all trucks traveling northbound side by side, one in each lane including shoulders

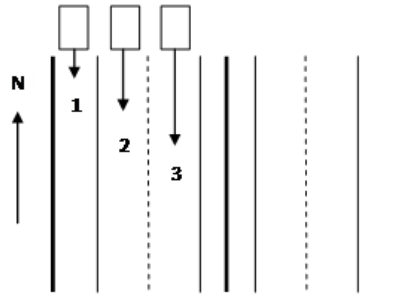
The previously described formations are detailed in Figures 12 to 17.

STAGE 1

Pass1 (1e): #2784

Pass2 (1a): #2677

Pass3 (1b): #2829



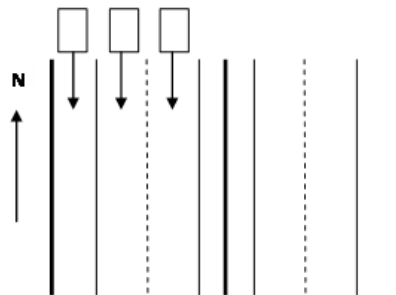
STAGE 2

Pass4 (3a):

Shoulder: #2969

Right Lane: #2771

Left Lane: #2758



STAGE 3

Pass5 (1f): #2784

Pass6 (1d): #2677

Pass7 (1c): #2829

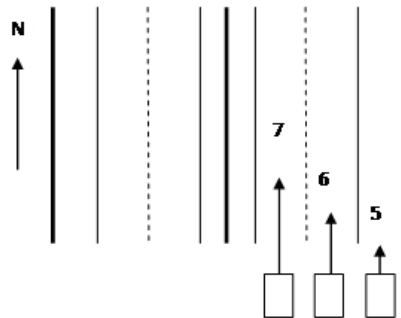


Figure 12 Test 2 Pass Diagrams, Stages 1 to 3

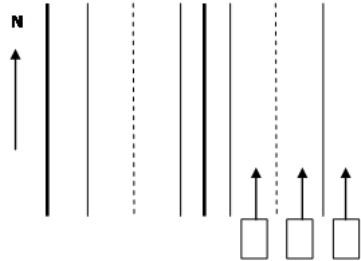
STAGE 4

Pass 8 (3b):

Shoulder: #2969

Right Lane: #2771

Left Lane: #2758



STAGE 5

Pass 9 (2g): East: #2677



West: #2784

Pass 10 (2a): East: #2758



West: #2829

Pass 11 (2b): Front: #2771



Rear: #2969

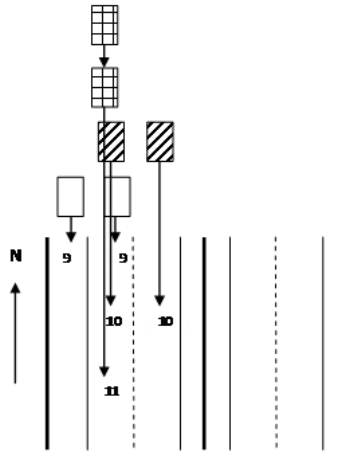
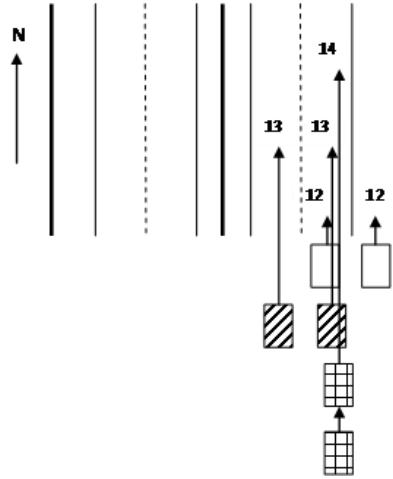


Figure 13 Test 2 Pass Diagrams, Stages 4 and 5

STAGE 6

- Pass 12 (2h): East: #2784
 West: #2677
- Pass 13 (2d): East: #2829
 West: #2758
- Pass 14 (2f): Front: #2771
 Rear: #2969



STAGE 7

- Pass 15 (2c): Front: #2784
 Rear: #2677
- Pass 16 (4b): Front West: #2829
 Front East: #2758
Rear West: #2969
Rear East: #2771

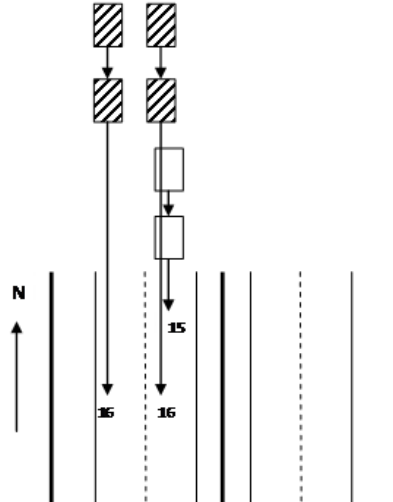


Figure 14 Test 2 Pass Diagrams, Stages 6 and 7

STAGE 8

Pass 17 (2e): Front: #2784



Rear: #2677

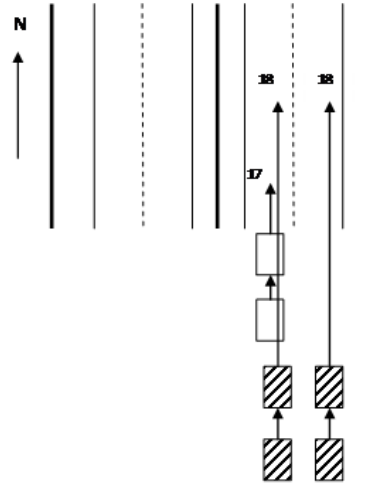
Pass 18 (4c): Front East: #2829



Front West: #2758

Rear East: #2969

Rear West: #2771



STAGE 9

Pass 19 (6a):

Position 1: #2784

Position 2: #2677

Position 3: #2829

Position 4: #2969

Position 5: #2771

Position 6: #2758

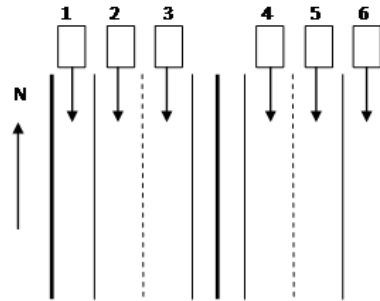


Figure 15 Test 2 Pass Diagrams, Stages 8 and 9

STAGE 10

Pass 20 (6b):

Position 1: #2758

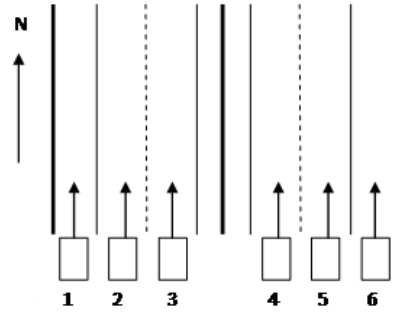
Position 2: #2771

Position 3: #2969

Position 4: #2829

Position 5: #2677

Position 6: #2784



STAGE 11

Pass 21 (4a):

Position 1: #2784

Position 2: #2677

Position 3: #2829

Position 4: #2758

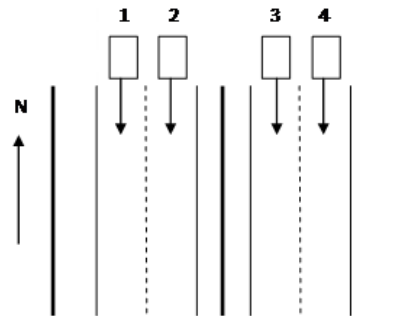


Figure 16 Test 2 Pass Diagrams, Stages 10 and 11

STAGE 12

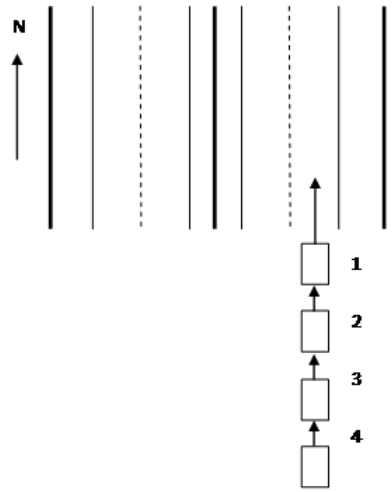
Pass 22 (4e):

Position 1: #2784

Position 2: #2677

Position 3: #2758

Position 4: #2829



STAGE 13

Pass 23 (4d):

Position 1: #2784

Position 2: #2677

Position 3: #2758

Position 4: #2829

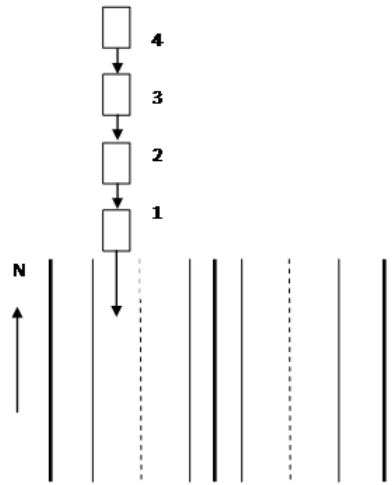


Figure 17 Test 2 Pass Diagrams, Stages 12 and 13

For the dynamic passes, four vehicles traveled both southbound and northbound across the span. These dynamic tests were conducted at approximately 55 mph with 100 foot intervals between the trucks at top speed:

Dynamic Truck Passes:

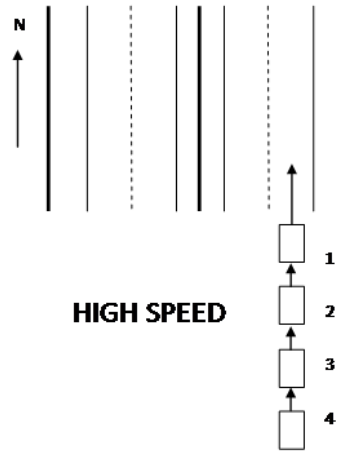
Pass #24 (4f): all trucks traveling northbound in succession, all in slow-lane

Pass #25 (4g): all trucks traveling southbound in succession, all in slow-lane

The previously described formations are detailed in Figure 18 as well.

STAGE 14

Pass 24 (4f):
Position 1: #2784
Position 2: #2677
Position 3: #2758
Position 4: #2829



STAGE 15

Pass 25 (4g):
Position 1: #2784
Position 2: #2677
Position 3: #2758
Position 4: #2829

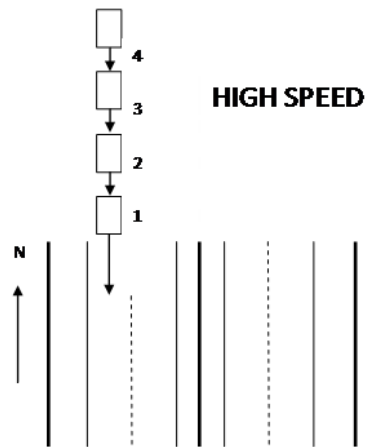


Figure 18 Test 2 Pass Diagrams, Stages 14 and 15, Dynamic Passes

Lastly, to possibly get an idea of how the load is shed across the bridge, a single truck was positioned transversely across the bridge and moved to different

locations at mid span. This was pass 26, the final pass of the load test, and can be seen in Figure 19.

STAGE 16

Pass 26:

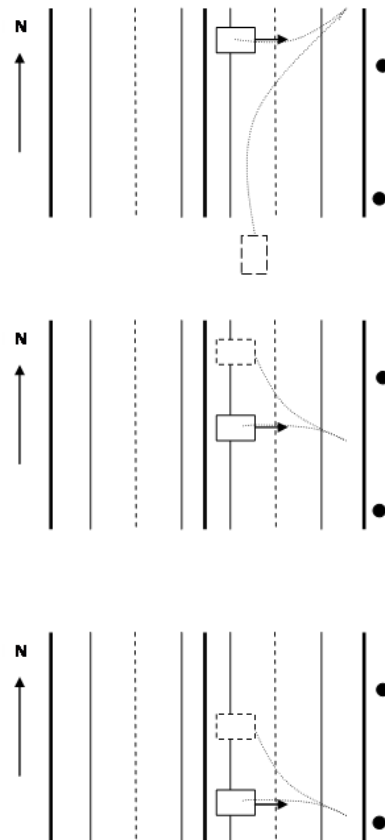


Figure 19 Test 2 Pass Diagrams, Stage 16, Transverse Placement

Chapter 4

TEST RESULTS

4.1 Analysis Method

From each load test there was an immense amount of data collected and processed. This was the case since one of the main purposes of these two load tests was to finally investigate for the first time the output of the system as well as determine how each sensor was reacting. This purpose deemed it necessary to look at the output of every single sensor out of the total 127 sensors and determine which data was valuable. The data from each pass was downloaded from the two Micron Optics model SM130 interrogators and saved as text files to be used. Later, this data was accessible through a cloud system connected from the bridge to the University of Delaware systems. These text files were then imported into Excel in order to be processed and examined.

Each individual pass constituted its own excel file to examine the data for all of the sensors. When taking the original data and plotting it, there was evident noise that obscured the runs, to the point of approximately ± 5 microstrain. To get a more accurate representation of the data collected, a “smoothing” process was used. This act of smoothing the data was done by taking a running average of 25 data points throughout the data. Along with this processing, the sensors output was zeroed using the first data point to mitigate any strain, displacement, or tilt felt in the sensor before the trucks affects were felt by the sensor. With the combination of these two actions being applied to all of the outputs from each sensor, especially the strain sensors, the created plots gave a great visual depiction of the effects of each truck formation pass.

Accelerometers were not investigated as thoroughly with this technique due to the varying affects the trucks had on these sensors as well as their uncertain status during testing. Peak values and any other values discussed in this investigation of data was taken from the smoothed data produced and was believed to me more accurate than the data including noise. All graphs were created in Excel to present this data. Every single file had graphs for every single sensor besides accelerometers to assist in determining if each sensor was functioning as expected. Any additional analysis method used in the following sections will be detailed in the section presenting that specific data.

Due to the immensity of the data, in retrospect a program such as MATLAB should have been used to process the data. At times Excel struggled because it can only hold 64,000 long data sets, making the data collected at 250 Hz too large of a data set to fit. Every other point was used for the sensors collected at 250 Hz so that their data could fit in its entirety. This was done for only the sensors we deemed necessary to investigate, primarily the strain sensors that were connected to the 250 Hz system. This higher collection rate's purpose, compared to 125 Hz, was to collect data from the accelerometers due to their sensitivity.

Additionally, opening and saving files took around five to ten minutes, making the use of Excel time consuming and impractical. Since individuals before me used Excel, I continued the tradition because of these previous experiences. It was realized too late into my work that a switch to MATLAB was imperative. As my work was completed we decided as a group to switch to MATLAB to increase efficiency and presentation of the data. This switch can be attributed to Nakul who has done intensive programming of the data processing codes that we now use. After

gaining more experience in MATLAB, I have conducted some analysis in the program as well.

4.2 Sample Results From Test 1

The results acquired from Test 1 were used in order to determine the baseline response for the IRIB. The following sections detail different areas of the test that were investigated.

4.2.1 Sensor Details

For this load test report, primarily strain sensors were focused on and investigated to determine different aspects about the bridge. The other gauges, which included, accelerometers, tiltmeters, displacement sensors, corrosion gauges and anemometers, were outside the scope of this load test. During future load test analysis, these gauges should be focused on as well.

The strain gauges during installation were actually attached to the steel rebar of the bridge in the desired section. It is assumed that the steel and the sensor have bonded completely to the concrete, so that both the steel and concrete are undergoing the same amount of strain. From this point, the respective modulus of elasticity is used to determine the stress in both the steel and concrete.

In this report, when it is said that the bridge at certain point is in tension, it is not actually in tension, but just in a lesser state of compression than before. Due to post tensioning and dead load stresses, tension never overcomes the compression in the bridge. There is no net tension in the bridge from the live load affects that were investigated in this load test.

4.2.2 Pass 4a's Use

For much of the discussion on this load test Pass 4a was used, which was when a single truck was in each lane, side by side, as they crossed the bridge. There were multiple reasons why this pass was used to investigate the responses of the bridge. The first was that this pass induced the highest strains seen in the bridge, giving the maximum loading condition from the test. As a result of these strains being the largest, the strain graphs of Pass 4a showed the most prominent changes and illustrated concepts the best. Additionally, the bridge behaves in a linear fashion, so that certain runs could be superimposed on one another to equal Pass 4a, giving Pass 4a governing authority over how the bridge behaves.

This process of superimposing can be examined by taking all the runs in which there was a single truck in a lane (Pass 1a, 1b, 1c, and 1d) and adding their strain data together and comparing this with the data from the pass where each lane had one truck (Pass 4a). First off an assumption is made that all of the sensors read their maximum strains when the trucks pass over their positions on the bridge, and these maximums are what were used for this calculation and all others throughout the report. This addition and comparison was done with every strain sensor along the deck and gave numbers that were close to one another at all positions except for sensors located where the pylons are. This is due to load from the truck going into the pylon as well as the deck at these points. An example of this comparison calculation with strain sensor S_E8 is as follows. When all the single passes were added together the total value was 86.42 microstrain ($\mu\epsilon$) while Pass 4a gave a result of 85.51 $\mu\epsilon$, illustrating a very similar response.

4.2.3 Peak Strains

The largest tensile strain recorded in the edge girders was 102 $\mu\epsilon$, at sensor S_W22 during Pass 4a. The following equation (1) was used to convert the fracture strength in compression (f^l_c) into a value for the modulus of elasticity.

$$E = 57,000\sqrt{f^l_c} \quad (1)$$

The f^l_c used for the edge girders in compression was 7210 psi, the average of the 56 day concrete breaks performed by DelDOT on edge girder concrete. For the concrete in tension a value of 0.08 of the f^l_c was used because concrete cracks from 0.1 to 0.15 f^l_c . In turn, the edge girder modulus of elasticity (E) used for concrete in compression was 4840 ksi while in tension it was 1369 ksi. The maximum tensile strain corresponds to a live load stress of approximately 140 psi in the concrete and a load of 2958 psi in the steel rebar that the sensor is attached to, using an E value of 29,000 ksi for the steel. The largest recorded compressive strain in the edge girders was 45 $\mu\epsilon$, at sensor S_W21 during Pass 4a as well and corresponded to a live load compressive stress of 218 psi in the concrete and a stress of 1305 psi in the rebar. The top of the edge girder primarily experienced compression and did not experience strains as large as the bottom gauges because the neutral axis of the sections is closer to the top than the bottom of the edge girder. This maximum value of 102 $\mu\epsilon$ was close to the governing location of the bridge, which was used for the load rating of the edge girder. However, the value of 102 $\mu\epsilon$ compared well enough with 97 $\mu\epsilon$, the maximum recorded strain at sensor S_W8 (middle of the bridge) during Pass 4a, allowing the center of the bridge to be where much of the further investigation occurs.

The largest tensile strain recorded in the pylons was 28 $\mu\epsilon$, at sensor S_W24S during Pass 4b while the largest compressive strain of 38 $\mu\epsilon$, was recorded at the same sensor during the Pass 4d. An E value for the pylons was calculated by using

an f^l_c value of 7696 psi, which was the average of the 56 day break concrete test performed by DelDOT on concrete used in the pylon. This makes the compressive E value for the concrete in the pylons 5000 ksi, while in tension (using $0.08 f^l_c$), the E value used was 1414 ksi. The tensile strain of $28 \mu\epsilon$ corresponds to a tensile stress of 39.6 psi in the concrete and 812 psi in the steel rebar, while the compressive strain of $38 \mu\epsilon$ corresponds to a compressive stress of 190 psi in the concrete and 1102 psi in the steel rebar.

All of the maximum and minimums from the load test were calculated and tabulated. Within these data tables every single pass was examined.

4.2.4 West to East Comparison

It is interesting to note that the east girder experiences lower strains than the west girder. This difference is due to a pedestrian walkway located on the eastern side of the bridge. Figure 20 shows a deck cross section of the bridge, illustrating the differences between the two sides. Due to the walkway, the eastern edge girder is further away from the applied load of the trucks, making the amount of load felt (and corresponding strains) smaller than the western side. There are also extra barriers (concrete and Jersey) along with the pedestrian walkway that act as stiffeners on the eastern side of the bridge. Therefore, the overall peak strains are experienced by bottom gauges of the western edge girder. For primarily all of the bridge characteristics investigated, the Western side's data was used because of the larger strain readings and the fact that it governs the performance of the bridge.

Teflon could have made the clamp slip around the rebar and made it so no reading could be acquired.

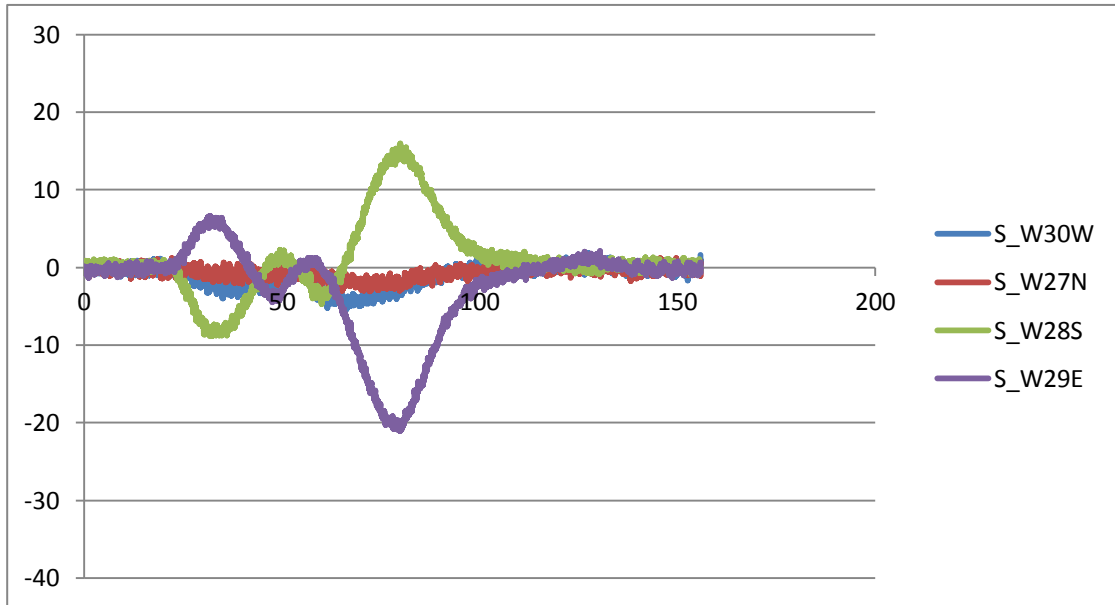


Figure 21 Mislabeled of Strain Sensor S_W29E (Seconds vs. Microstrain)

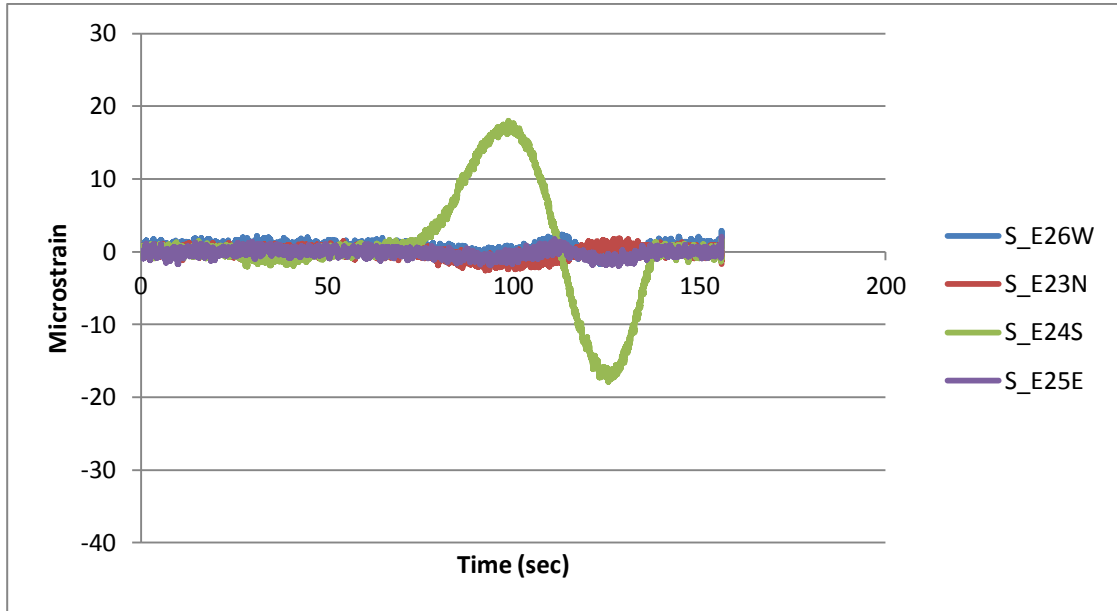


Figure 22 Floating Sensor S_E23N (Seconds vs. Microstrain)

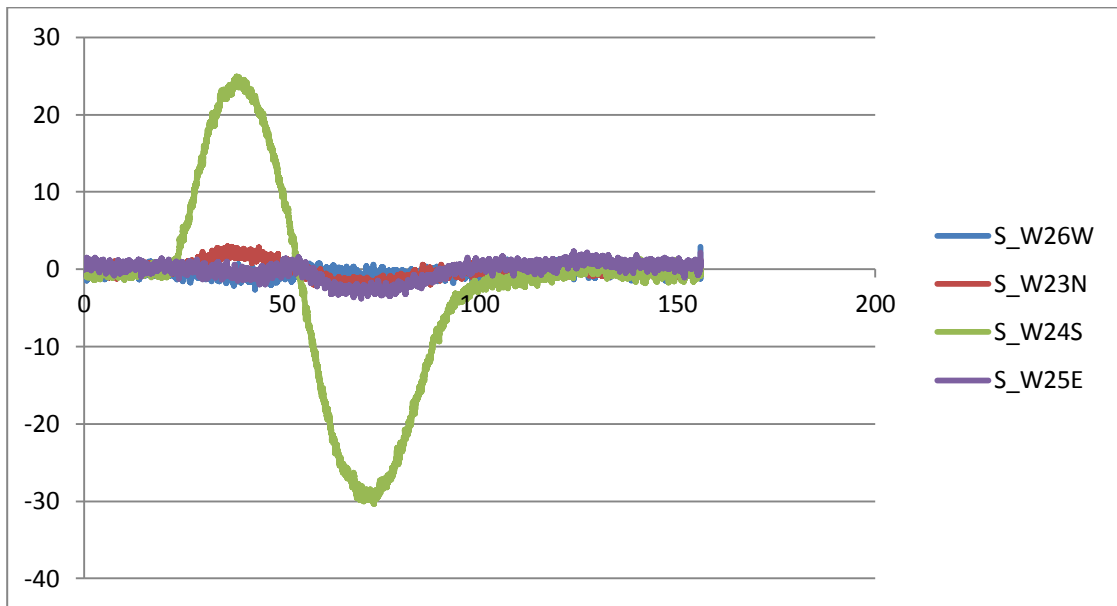


Figure 23 Floating Sensor S_W23N (Seconds vs. Microstrain)

Top and Bottom Array Behavior

There is a difference in response between the top and bottom arrays of strain sensors in the pylons. The bottom arrays of sensors experience larger, more gradual strain, concentrated mostly in the southern and northern sides of the pylon. This reaction can be seen in Figure 24. The top arrays of sensors experience smaller, more variable strains in the north and south directions which can be seen in Figure 25. It could be thought that the top may be more variable and sways as the loading damps over time.

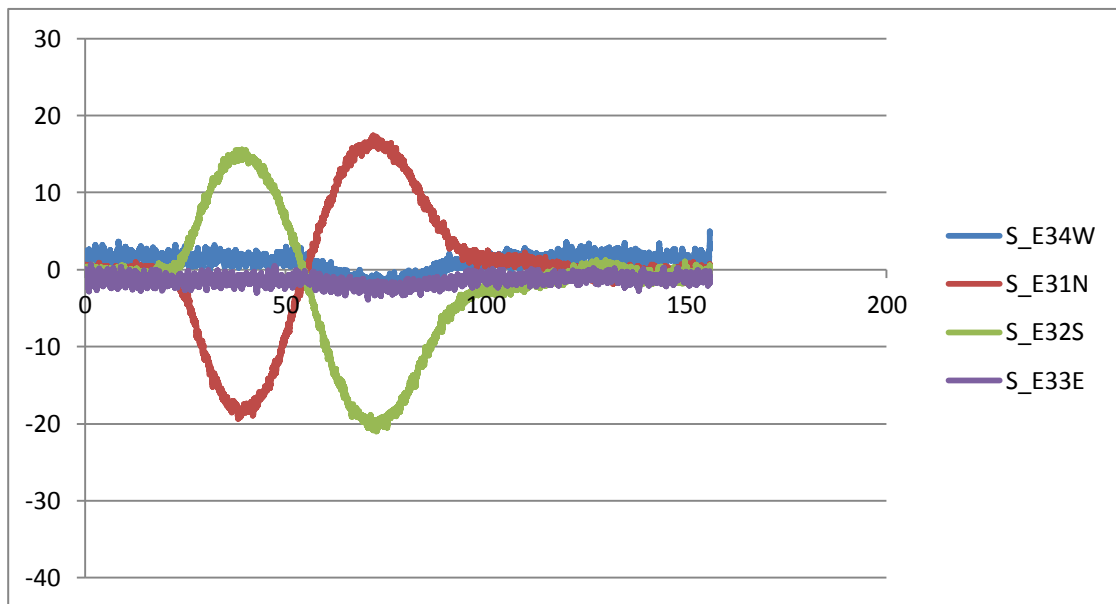


Figure 24 Bottom Array Pylon Strain (Seconds vs. Microstrain)

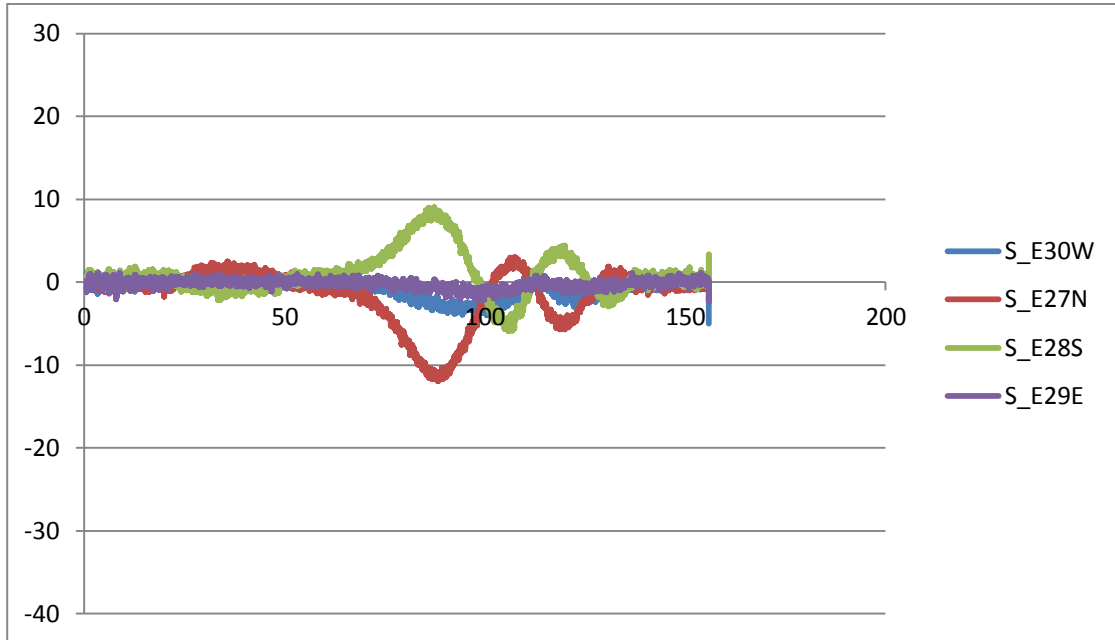


Figure 25 Top Array Pylon Strain (Seconds vs. Microstrain)

Reverberation in the Pylons

This reverberation was looked at more in depth to see if it was just an action of damping out load over time. Figure 26 was used to show the movement of the trucks across the bridge over time to help investigate this phenomenon and many of the other characteristics of the bridge. Looking at the southeastern pylon's upper strain sensor array (Figure 25), the pylon behaves unexpectedly. By looking at the southern side of the pylon's strains you can see this. At 85 seconds, when the truck is in the middle of the bridge, there is a maximum amount of tension (normal), then at 105 seconds, the truck is almost at the pylon there is compression in the sensor (still should be tension). At 118 seconds, the trucks have passed the pylon and there is tension (you would think compression). Then at 145 seconds (using a kinematic equation to determine it takes 113 seconds to cross), the truck is moving off the

bridge, and there is compression (normal). This exhibits almost like a damping effect in the pylons from the stays. Only the top stays connect at the middle of the bridge and are only affected when the truck is there. After the truck leaves the area of the top pylon stays, the pylon is unaffected and needs to damp it out. This idea comes from how the max strain times do not correspond with truck positions.

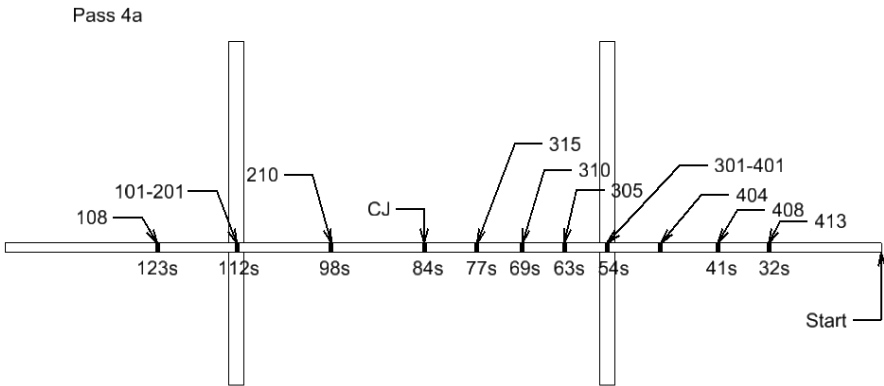


Figure 26 Truck Movement Across Bridge

The reverse phenomenon happens at the Northwestern pylon upper array (Figure 27). It seems as though when the truck approaches the pylon from the north, the top of the pylon begins swaying from the load. When the truck passes the pylon and reaches the center of the bridge, there is the maximum in strain shown through a

larger spike in the data. Once the truck gets off that half of the bridge, the pylons become inactive because they no longer experience load.

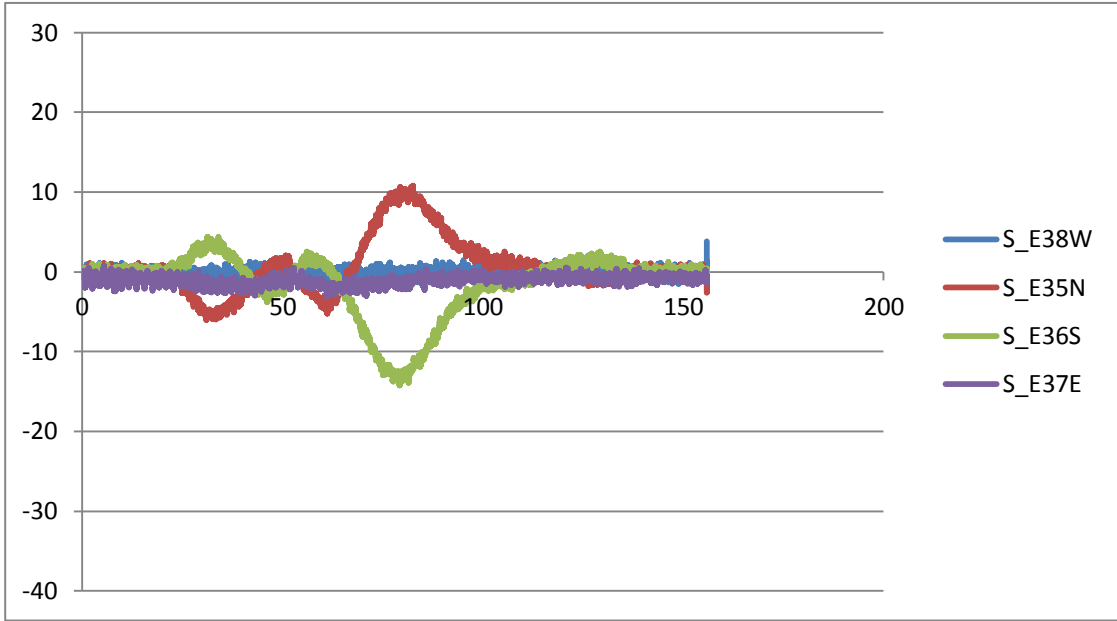


Figure 27 Top Array Strain, Northwestern Pylon (Seconds vs. Microstrain)

This response is unexpected because when the truck was on the north side of a pylon, the southern side should be in tension in the upper arrays the whole time (this would be because there should be a resultant force to the north through the cable stays). When the bridge crosses the pylon it would be thought that the resultant force in the stays would be to the south so that the southern side would be in compression. Overall, this was a reoccurring phenomenon that could not be fully explained from just this baseline load test, but could possibly happen as a result of forces in the cable stays. These forces could be examined by looking more in depth at this response.

4.2.6 Most Extreme Loading Conditions

There are certain times and positions that the most extreme loading conditions occurred while the trucks drove across the bridge. After inspecting the graphs it seems like moderately extreme conditions are at the 40 second, 70 second, and 100 second marks. Figure 26 shows the truck positions that correspond with these times. This can be said because of the strain readings in both the pylons and edge girders at these instances. To rank how extreme each condition was, each edge girder sensor's position was investigated at the time the truck went over it as well as with the pylon strains at that time. The most extreme loading conditions were determined by a process of looking at the graphs and their times and then adding the strains together at each individual time. The times with the highest combined strain readings from the edge girder and the pylon were deemed the worst positions for the truck to be. The positions when the trucks were about halfway to the first pylon (Joint 408), $\frac{1}{4}$ onto the main span (Joint 310), and $\frac{3}{4}$ onto the main span (Joint 210) were when the moderately extreme loading conditions occurred.

The overall most extreme loading condition was when the trucks passed over the cross joint located mid span of the bridge at around 85 seconds. Here strain gauges 7 and 8, both east and west, read their maximum amounts for the run. In the majority of the pylons there is strain being recorded at this time, ranging from a more minor amount, to a few maximums at this time. Also there is strain in the other edge girder gauges away from the middle of the bridge due to the presence of the trucks, creating negative bending in those portions. This makes sense that this would be where the most strenuous loading would occur because it is in the middle of the bridge and at the furthest position away from the pylons and stay cables. This creates a maximum bending moment in the pylons along with a maximum compressive force on

the edge girders due to the trucks being at the greatest distance away from the pylons, which take their lowest axial loading at this time.

4.2.7 Strain in Pylons

The maximum strain in the pylons, which would be if all the truck weight went into a single pylon at one time, was calculated. This was done by acquiring the modulus of elasticity of the concrete while in compression by using equation (1). The value of f^1c used for the pylons was 7696 psi, which was the average of the 56 day break concrete test performed by DelDOT on concrete used in the pylon. By using this value, the E value for the concrete in compression was determined to be 5000 ksi. This was then used in conjunction with Hooke's Law, the cross sectional area of a pylon, and the maximum applied load of 256 kips (4 trucks) to get the strain in the pylon. This value in all cases was miniscule, never getting to be more than $4.67\mu\epsilon$. The main value that should be investigated was the one that came from the cross section of the array beneath the deck on the south eastern pylon (S_E26W, S_E23N, S_E25E, S_E24S). This is because at this location there would be strain due to an applied load on the deck because of its position under the deck. A cross section of this area is shown with Figure 28. The strain value at this location would be $2.7\mu\epsilon$, a very small amount. Since such a low strain value would come from the axial force of the four trucks, it can be determined the strains experienced in the pylons are due to bending moments and not axial forces.

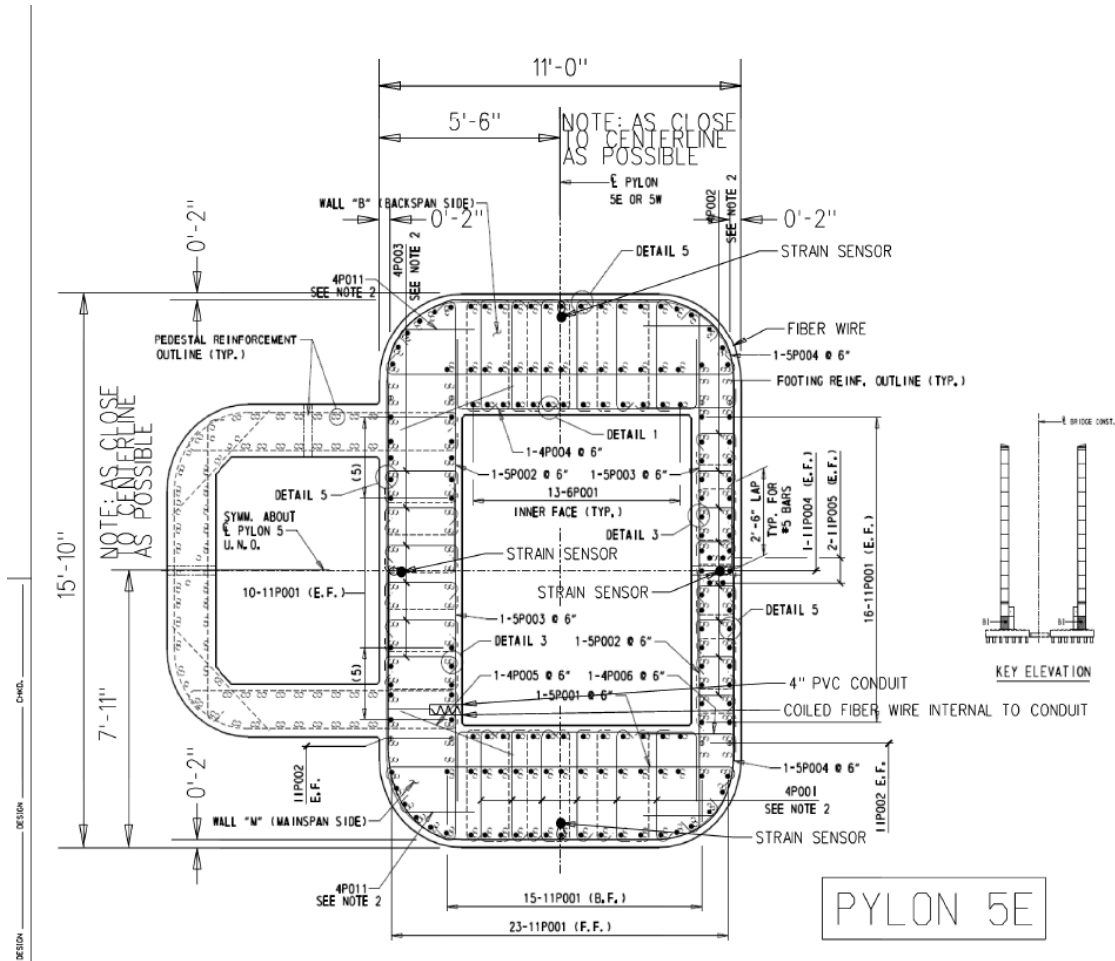


Figure 28 Pylon Cross Section Underneath Deck

4.2.8 Fundamental Frequency

In order to determine the fundamental frequency of the bridge, the responses due to the dynamic load Pass 4f were examined. This pass did not induce sufficient vibrations in the accelerometers so they could not be used in evaluating the bridge’s fundamental frequency. Instead, strain gauges on the edge girders were examined. Only the strain gauges in tension, or on the bottom of the edge girder, were used because they had prominent enough readings. Additionally, strain gauges 4 and 16

(both east and west) were excluded because these gauges are located at the pylon, which reduced vibrations. After the trucks passed over strain gauges, a vibration was induced that could be seen in the strain gauge readings. The portion of the response that was examined corresponded to the time from when the loaded truck train completely passed over the gauge to the end of the pass. This portion of data was demeaned and then put through a Fourier Transform to determine the linear fundamental frequency of the bridge. Based on the analysis, the fundamental frequency was 0.244 Hz (cycles per second). This process can be seen in Figures 29 to 31 which are all strain data for sensor S_W8 from 105 seconds to the end of the run. Figure 29 is the unsmoothed strain versus time data, Figure 30 is the data that has been demeaned, and Figure 31 is the acceleration versus frequency data that is acquired after performing the Fourier Transform on the demeaned data. The value of 0.244 Hz corresponds well with a study done on the Bill Emerson cable stayed bridge that had a fundamental frequency of 0.34Hz (Chen 2006). Additionally, the *Bridge Engineering Handbook's* portion on cable stayed bridges by Man-Chung Tang states that cable stayed bridges should typically have fundamental periods of 3 seconds or longer (Tang 1999). The Indian River Inlet Bridge would have a 4.09 second fundamental period, which agrees well with what is expected.

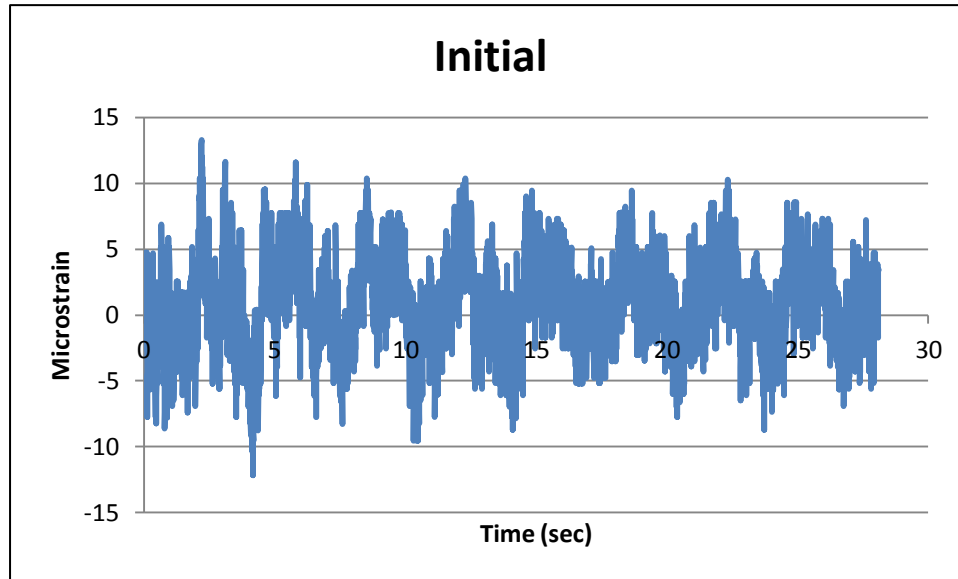


Figure 29 S_W8 Initial Data from 105 Seconds to End of Time Series

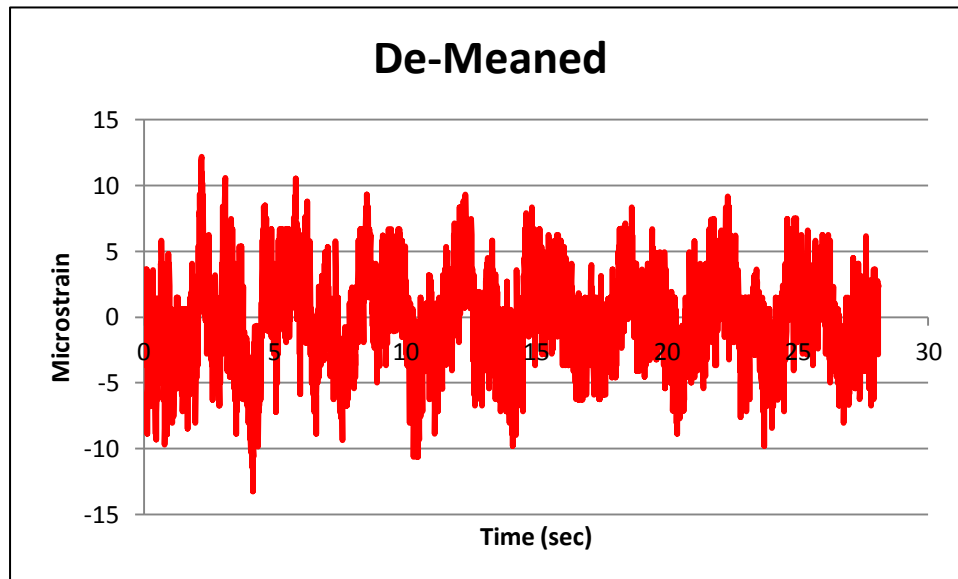


Figure 30 S_W8 Demeaned Data from 105 Seconds to End of Time Series

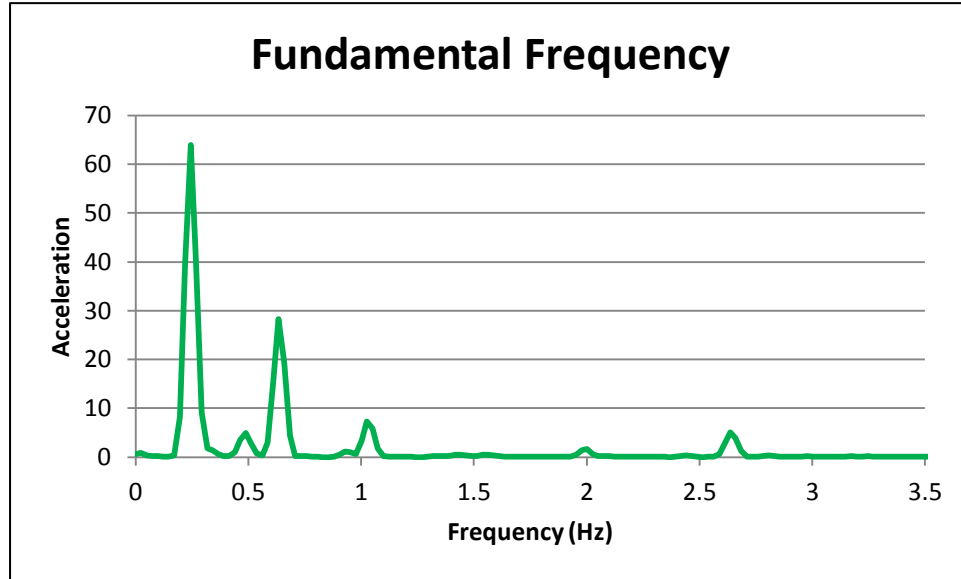


Figure 31 S_W8 Fundamental Frequency

4.2.9 Transverse Load Distribution

Transverse load distribution across the bridge was investigated by looking at a single truck as it went across the bridge in each of the four lanes. The passes that place one truck in a lane are Passes 1a, 1b, 1c, and 1d. This helps develop an idea of how much load a single edge girder may take as a truck is moved across the bridge transversely. By using measurements of how wide the bridge deck is, a graph was created plotting the percentages of loading from the western edge girder of the bridge. This graph includes data from strain sensor S_W8 and appears as Figure 32. The graph will help determine where exactly a truck appears on the bridge by taking the maximum strain reading from sensor S_W8 and dividing that by the total strain at that cross section ($S_{W8} + S_{E8}$). The total strain at the cross section is the strains from the east and west sensors added together and then averaged over the 4 passes. This value turned out to be 47.6 microstrain. This gives the percentage of loading and will

allow for an exact location transversely of the truck to be determined by examining the graph.

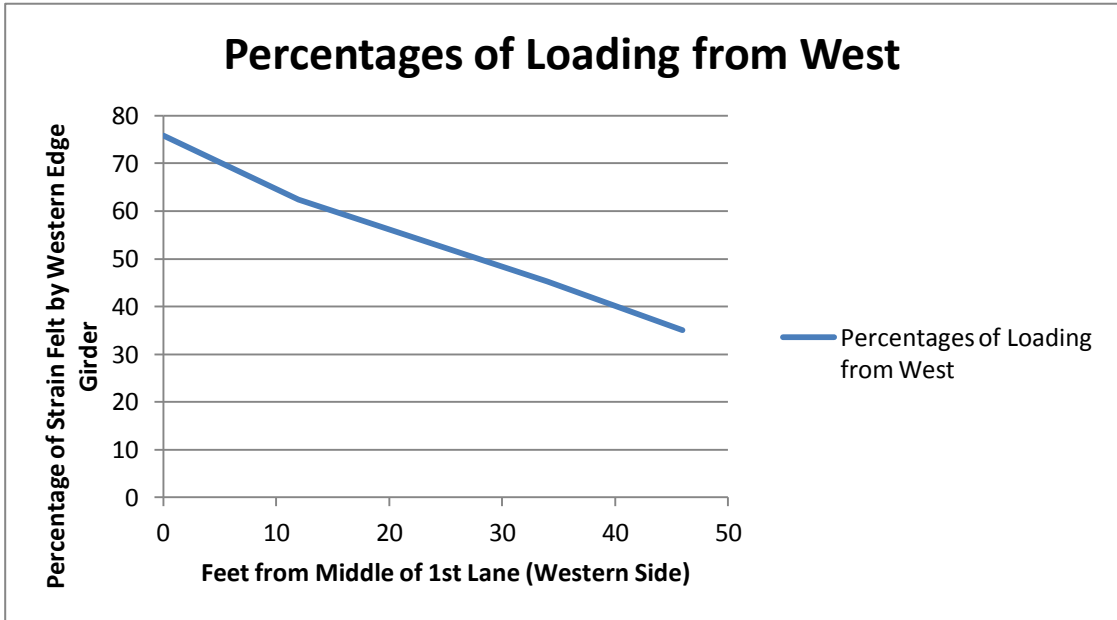


Figure 32 Percentages of Loading Using S_W8, Truck Moving Transversely West to East

4.2.10 Distribution Factors

The distribution factors were calculated for the bridge by examining strain data and the percentage of loading from the western side using strain gauge S_W8. Each factor was calculated with respect to one truck and the amount of strain that it created in both the eastern and western side strain gauges at the same cross section of the deck. The distribution factors for 1 truck per lane are given in Table 1. The single truck distribution factor for one lane, 0.758, shows that when a single truck is loaded in the westernmost lane, 75.8% of the load is held by the western edge girder. In

conjunction with these distribution factors, a multiple presence factor could be added to illustrate the actual probability of the 3 and 4 lane loading occurring. Additionally, in Table 2, distribution factors for a two truck train were calculated across the bridge, ending with a factor that illustrates if there were 8 trucks on the bridge at once. Lastly, in Table 3, a four truck train's factors were calculated with a maximum of 16 trucks on the bridge at once. The values of the two truck and four truck trains are similar showing that the loading has the ability to spread out across the bridge.

Table 1 Distribution Factors for One Truck Per Lane

| Lane # (West to East) | Distribution Factors | Passes Used | Single Truck Distribution Factors (4 Trucks across) |
|-----------------------|----------------------|-------------|---|
| 1 | 1 Lane | Pass 1a | 0.76 |
| 2 | 2 Lanes | Pass 1b | 1.38 |
| 3 | 3 Lanes | Pass 1c | 1.83 |
| 4 | 4 Lanes | Pass 1d | 2.18 |

Table 2 Distribution Factors for a Two Truck Train Per Lane

| Lane # (West to East) | Distribution Factors | Passes Used | S_W8 (2 Truck Train Run) | 2 Truck Train Distribution Factors (8 Trucks across) Divide by 1 Truck |
|-----------------------|----------------------|-------------|--------------------------|--|
| 1 | 1 Lanes | Pass 2b | 56.6748 | 1.19 |
| 2 | 2 Lanes | Pass 2c | 48.47008 | 2.21 |
| 3 | 3 Lanes | Pass 2e | 38.08012 | 3.01 |
| 4 | 4 Lanes | Pass 2f | 29.32728 | 3.63 |

Table 3 Distribution Factors for a Four Truck Per Lane

| Lane # (West to East) | Distribution Factors | Passes Used | S_W8 (4 Truck Train Run) | 4 Truck Train Distribution Factors (16 Trucks across) Divide by 1 Truck |
|-----------------------|----------------------|-------------|--------------------------|---|
| 1 | 1 Lanes | Pass 4d | 64.76984 | 1.36 |
| 2 | 2 Lanes | | 53.28127048 | 2.48 |
| 3 | 3 Lanes | | 38.61084219 | 3.29 |
| 4 | 4 Lanes | | 29.92255539 | 3.92 |

4.3 Comparison of Two Tests

The main goal of conducting the second test was to be able to compare it to the April 2012 test, giving an overview of the repeatability and the consistency of the response of the bridge.

4.3.1 Compare Peak Response

The first step was to compare this November (Test 2) load test to the one that took place in April (Test 1) to determine the repeatability of the results acquired. To do so, the percent differences between the tests were calculated by taking the results of the November test, subtracting it by the April test and then dividing the whole quantity by the April test value. This is shown by the following equation (2).

$$(2) \frac{LT2 - LT1}{LT1} * 100$$

This calculation was done for passes 1a-1d, 2a-2f, and 4a-4e, due to these all being included in both the April and November load tests. The dynamic passes, 4f and 4g, were excluded because of the variability created by the speed of the trucks crossing the bridge. The positive maximum from each pass for certain sensors were

used as the values in the equation. In order for the percent difference to be a meaningful calculation, the sensors had to read a moderate maximum strain reading for every pass. This minimum value for all passes was 10 microstrain. The sensors that met this requirement for all passes were S_E8, S_E22, S_W2, S_W8, S_W10, S_12, and S_W22. Additionally, sensors S_C1's and S_C2's percent differences were calculated because they only read compressive (negative) strains due to their placement in the bridge deck, but still had large enough magnitudes to be of significance. The results of this calculation are tabulated in Table 4. For all the sensors besides S_C1 and S_C2, a negative percent difference means a decrease in strain from Test 1 to Test 2, while for S_C1 and S_C2, a positive percent difference means a decrease in strain from Test 1 to Test 2 due to using minimum values instead of maximums. Overall, the minimum percent difference was 0% from sensors S_C1 during pass 2a, while the maximum was 31.6% from sensor S_C2 during pass 2d. The average of the absolute value of the percent differences was 9.82%.

Out of all the sensors, the best one to investigate was S_W22 because of its location so close to the controlling point of the bridge and also the fact that the overall maximum readings from all passes come from this sensor. The absolute maximum percent difference from sensor S_W22 was 20.7% from pass 2f while the minimum was 1% from pass 1b. The average percent difference for S_W22 was 10.9% with a standard deviation of 6.3%. These values show that the results from Test 1 and Test 2 are close to one another and illustrate that there is repeatability between load tests.

Table 4 Percent Difference in Response from April to November Load Test

| Strain Sensor | S_E8 | S_E22 | S_W2 | S_W8 | S_W10 | S_W12 | S_W22 | S_C1 | S_C2 |
|---------------|-------|-------|-------|-------|-------|-------|-------|-------|-------|
| Pass 1a (%) | -9.2 | 1.8 | -3.6 | -9.1 | -4.8 | -4 | -6.8 | -9.8 | 4.3 |
| Pass 1b (%) | -10 | -13.8 | 0.8 | -6.3 | -5.8 | 3.4 | 1 | 1 | -7.3 |
| Pass 1c (%) | -5.5 | -5.7 | 2.4 | 1.4 | -10.1 | -9.4 | -11.1 | 7.3 | -14.7 |
| Pass 1d (%) | -1.6 | -11.3 | -1.8 | -4.6 | -9.9 | 9.2 | -14 | -0.6 | -9 |
| Pass 2a (%) | -6.9 | -13.5 | 0.4 | -7.2 | -3.7 | -4.8 | -10.2 | 0 | -4.5 |
| Pass 2b (%) | -14.7 | -16.1 | -17 | -19 | -26.5 | -20.3 | -16.7 | -14.3 | -14.6 |
| Pass 2c (%) | -14.1 | -19.3 | -6.2 | -14.4 | -17 | -16.5 | -20.3 | -14 | -12.4 |
| Pass 2d (%) | -3.1 | -4.3 | -2.9 | -8.1 | -9.8 | -18.1 | -13.1 | -18.7 | -31.6 |
| Pass 2e (%) | -14.9 | -12.9 | -16.5 | -19.4 | -20.3 | -23.8 | -17 | -16.3 | -28.4 |
| Pass 2f (%) | -17.5 | -22.3 | -9.2 | -8.3 | -11.8 | -14.4 | -20.7 | -8.9 | -26.9 |
| Pass 4a (%) | -8.1 | -9.7 | -1.8 | -6.8 | -5 | -3.8 | -10.8 | 0.4 | -6.4 |
| Pass 4b (%) | -8.1 | -2.8 | -6.1 | -7 | -11.1 | -6.1 | 1.6 | -3.4 | -14 |
| Pass 4c (%) | 1.9 | 8.8 | 14.5 | 0 | -1.5 | 3.2 | -2.6 | -10.4 | -16.1 |
| Pass 4d (%) | 7.4 | -14.1 | 9.1 | 2.1 | 1.2 | 8.8 | -11.2 | 20.8 | 31.2 |
| Pass 4e (%) | -0.6 | -2.9 | 14.5 | -1.3 | 6.5 | 14.3 | -7 | -1.5 | -2.9 |

4.3.2 Compare Similar Passes

There are a few comparisons that can be made with individual passes that are worthwhile to investigate. The first is a comparison between the April and November load test, focusing on pass 4a and sensor S_W22. This is a quality focus point due to

the intense investigation of pass 4a in the April load test report and because sensor S_W22 gives the largest response due to its proximity to the bridge's controlling point. Pass 4a, sensor S_W22, for April and November are plotted in Figure 33. The maximum value for April was 102 microstrain while the maximum for November was 91.1 microstrain. This shows a decrease in strain induced in sensor S_W22 from the first to the second test. This 10.6 % decrease could have been caused by many things, which are discussed in the next section. The graphs show that the edge girder exhibits the same pattern of positive and negative bending as the trucks approach, cross the sensor, and continue along the bridge. There is an offset in the plots due to differences in time histories and the length of data collection. Overall, there is a slightly lower peak strain value in the 2nd test, which indicates the bridge is behaving nominally and does not have any damage issues. This is because if it was damaged between the two tests, there would be much larger strains in the second test compared to the first.

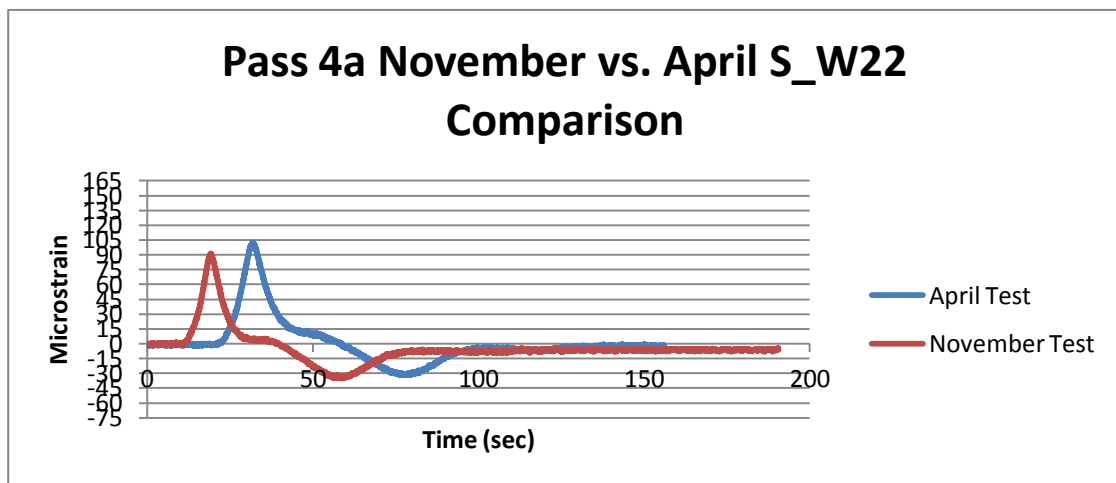


Figure 33 April vs. November Pass 4a Comparison

The second worthwhile comparison to examine is one between pass 4a and pass 6a from the November load test. Pass 4a induced the largest response in the April test while a formation like pass 6a created the largest response during the November test. As stated before the maximum microstrain in sensor S_W22 due to pass 4a was 91.1 microstrain while the maximum value read by pass 6a was 149 microstrain. The plot of these two passes can be seen in Figure 34. The same pattern of negative and positive bending can be seen in both of the responses, just with a much larger spike for pass 6a, which would be expected. The principle of superposition can be used while looking at pass 6a by adding the maximum response from S_W22 for each single truck pass. All 6 single truck passes' maximums in sensor S_W22 can be added together to see how close they come to the maximum response from pass 6a. The value when all the single passes have been added is 135.5 microstrain, which compares well with the actual value of pass 6a, 149 microstrain. The actual maximum response from the November test was from pass 6b, just 6a in the opposite direction, which was 151 microstrain.

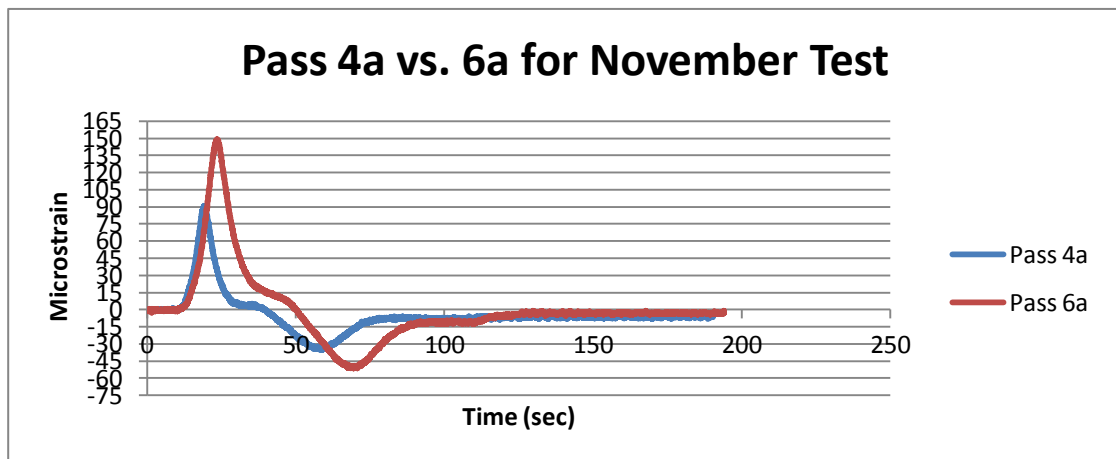


Figure 34 April Pass 6a Compared to November Pass 4a

4.3.3 Compare Load Distribution

Transverse load distribution across the bridge was investigated by looking at a single truck as it went across the bridge in each of the four lanes, as well as the shoulders in the November test. The passes that place one truck in a lane or shoulder are Passes 1a, 1b, 1c, 1d, 1e, and 1f. This helps develop an idea of how much load a single edge girder may take as a truck is moved across the bridge transversely. By using measurements of how wide the bridge deck is, a graph was created plotting the percentages of loading from the western edge girder of the bridge. This graph includes data from November's strain sensor S_W8 and appears as Figure 35. The graph will help determine where exactly a truck appears on the bridge by taking the maximum strain reading from sensor S_W8 and dividing that by the total strain at that cross section from that particular pass ($S_{W8} + S_{E8}$). The total strain at the cross section is the strains from the east and west sensors added together for a single pass. On average, one truck induces 45.2 total microstrain at the cross section. This gives the percentage of loading and will allow for an exact location transversely of the truck to be determined by examining the graph.

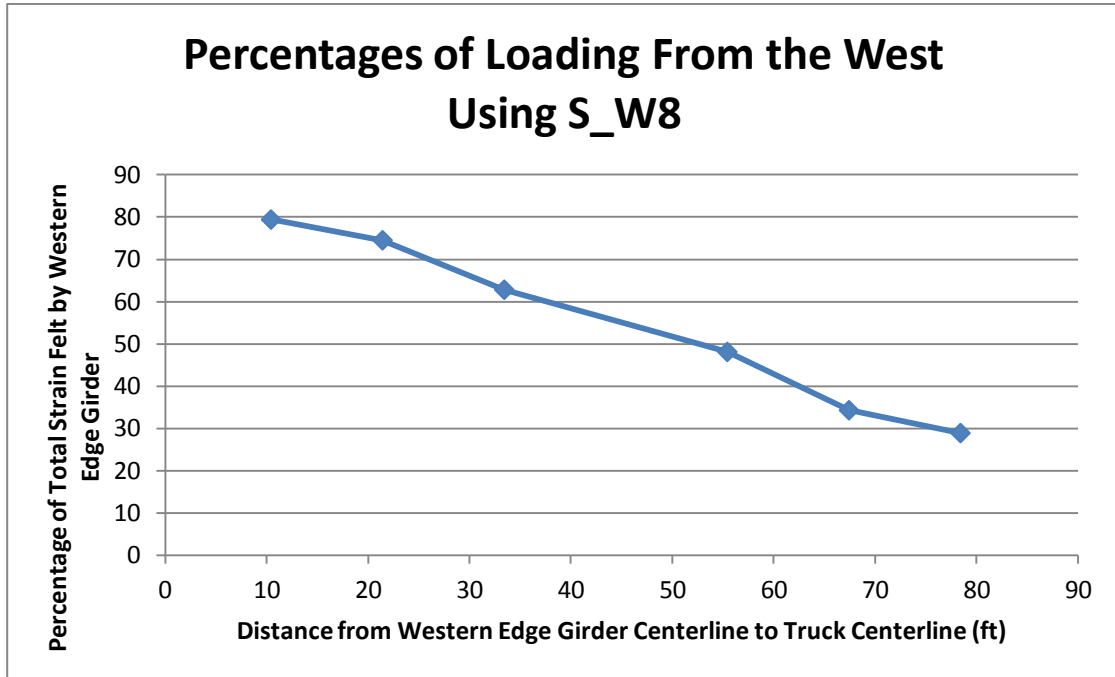


Figure 35 Test 2 Transverse Load Distribution at S_W8

Additionally, consistency of the tests can be examined by using the transverse load distribution from the April load test and overlaying it on top of Test 2's data. In Figure 36 it can be seen that the previous test's results (Red) compare well with the November test (Blue). Both lines' slopes match closely with one another and there is only an average percent difference between data points from the lane positions of 2.73%. To check to see if the bridge reacts consistently at a different point on the span, another location was investigated as well. Figure 3 shows the transverse flow across the bridge for sensor S_W6 from Test 2 data. This distribution from S_W6 is consistent with that of S_W8 and shows that at another point on the bridge the same load shedding occurs. There is an average 3.59% percent difference between each point when comparing S_W6 and S_W8.

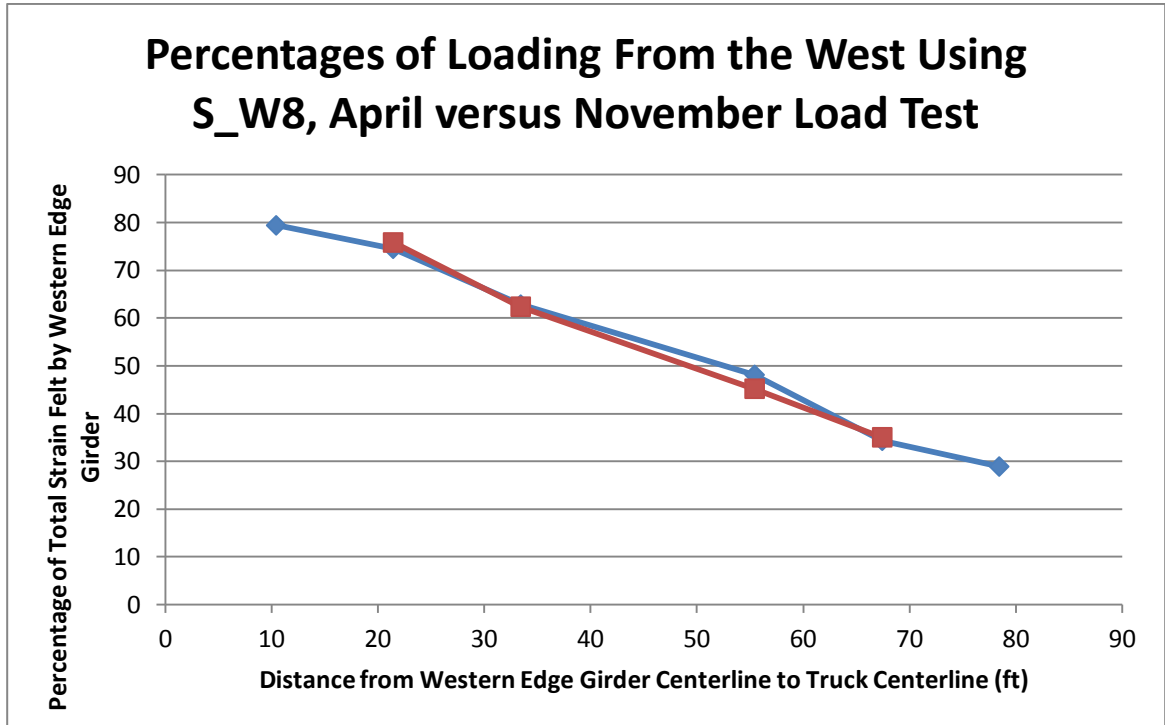


Figure 36 Transverse Load Distribution at S_W8 of Test 1 (Red) Compared to Test 2 (Blue)

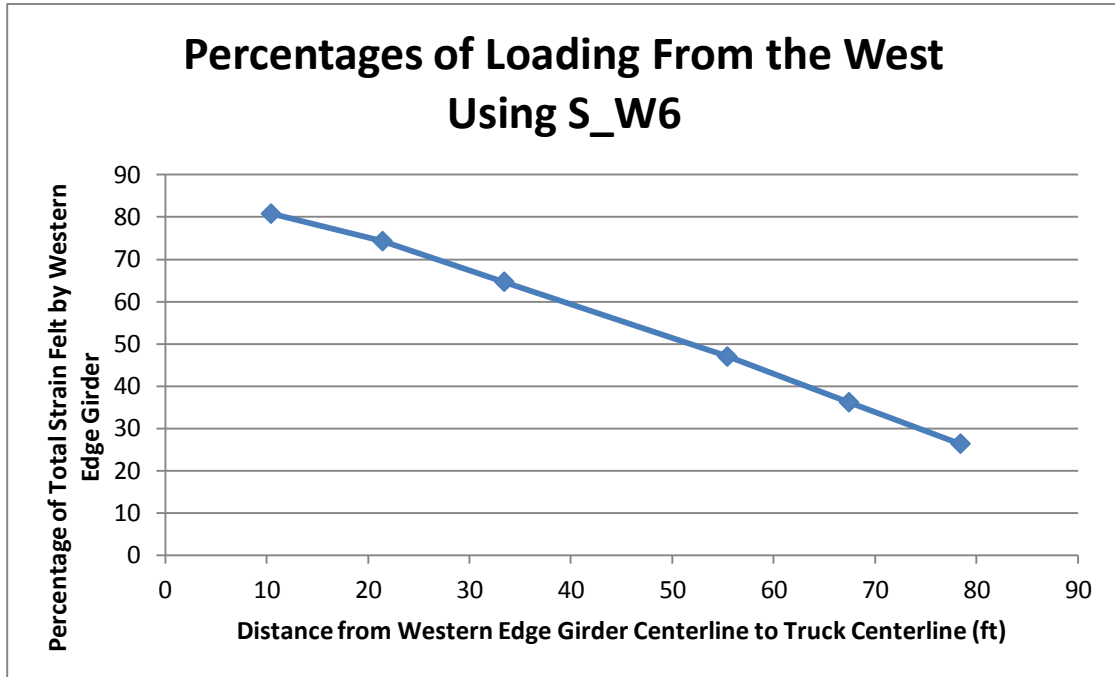


Figure 37 Test 2 Transverse Load Distribution from S_W6

This pattern for transverse load distribution is seen even far away from sensors S_W8 and S_W6. Figure 38 shows the distribution created by sensor S_W2. There is an average percent difference between data points from sensor S_W8 and sensor S_W2 that is 5.6 %, showing the close correlation that appears throughout the bridge.

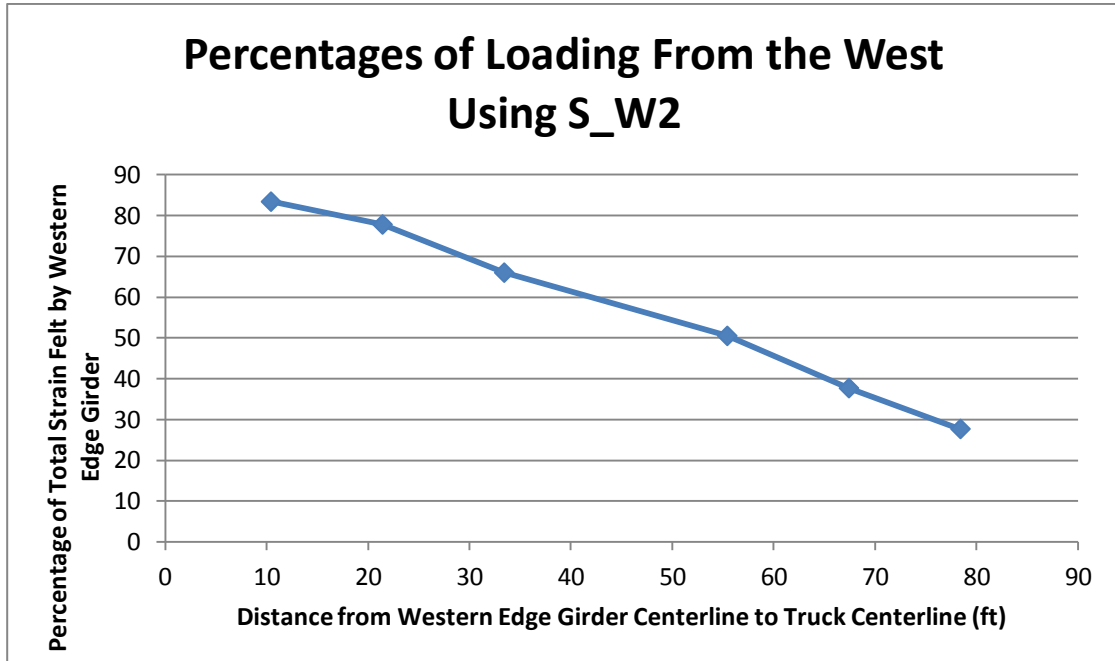


Figure 38 Test 2 Transverse Load Distribution from S_W2

4.3.4 Variability Discussion

There are many different possible explanations for why the April and November load tests do not generate responses with identical magnitude in the sensors. First off, the trucks used are slightly different weights in both tests. Table 5 lists the trucks, their weights, the average truck weight for both tests, and also their standard deviation. Lastly, there is a calculated percent difference between the two tests' average truck weights that is -1.7%. This value is negative due to the average truck weight of the April test being greater than the November test. Additionally, since this percent difference is small between each of the tests truck weights, there will only be slight changes in responses in the sensors. This slight change is exhibited in Table 4 that was detailed previously. No factors need be applied due to the small

percent difference of the averages of -1.7% and values would be expected to be around 1 to 2 % smaller in the November test due to the lighter load.

Table 5 Truck Weight Comparison by Test

| April Test | | | | November Test | | | | |
|------------|---------------|----------------|--------------------|---------------|---------------|----------------|--------------------|-----------------------------------|
| Truck # | Weight (kips) | Average (kips) | Standard Deviation | Truck # | Weight (kips) | Average (kips) | Standard Deviation | Percent Difference of Average (%) |
| 2829 | 63.2 | 63.5 | 0.222 | 2969 | 62.5 | 62.4 | 0.66 | -1.7 |
| 2677 | 63.7 | | | 2829 | 63.2 | | | |
| 2784 | 63.4 | | | 2784 | 62.4 | | | |
| 2904 | 63.6 | | | 2758 | 61.2 | | | |
| | | 2771 | 62.4 | | | | | |
| | | 2677 | 62.7 | | | | | |

There are other reasons that could have contributed to the differences in magnitudes seen by the strain gauges. Between the first and second test there were 7 months of time that passed. Since the IRIB was recently completed, during these 7 months, the concrete could have cured and hardened even more, giving various portions of the bridge different strengths. Truck position and speed also could have an effect on the response. Truck position transversely across the bridge could either decrease the response in an edge girder if it is further away or increase the response if it is closer. Also, the alignment of the trucks in their formations could not have been exactly like they were in the previous tests due to driver and speed differences.

Chapter 5

AMBIENT RESPONSE VERSUS LOAD TESTS

5.1 Temperature Induced Response

A goal of examining everyday traffic is to determine when to actually collect data on the bridge at a high rate or to know when there is an abnormally large strain reading that could indicate damage. In order to know when data should be collected, a trigger needs to be set that is a threshold strain amount. When the strain in an edge girder goes above this certain threshold, the system begins to run and collect data. The difficult part about setting this threshold strain is the fact that temperature fluctuates throughout the day as well as seasons, inducing strain in the sensors. The following section is an attempt to create a function that takes the temperature at an instant and converts it to a strain induced in the sensor from temperature. This would allow for the strain sensor to be zeroed at any instant, eliminating strains in the gauge from temperature, allowing only load induced strains to be seen.

5.1.1 Time History Investigated

In order to determine a function that would allow us to calculate strain induced in the sensor due to temperature at the time, a data set in which good fluctuations in temperature occurred was needed. The data that was investigated was the time history of strains and temperature over the ten day period from midnight August 10th, 2013 to midnight August 20th, 2013. Figure 39 is a plot of time versus both temperature and induced strains in strain sensor S_W8. Strain sensor S_W8 was used due to its

location at the center of the bridge and its smaller embedment depth into the bridge, which contributed to its nice fluctuations in strain in regards to temperature and time of day. The temperature on this plot is relative temperature compared to the first point on August 10th. At midnight on this day the temperature was 74.2 degrees Fahrenheit according to the Delaware Environmental Observing System (DEOS) at the Indian River Inlet weather station.

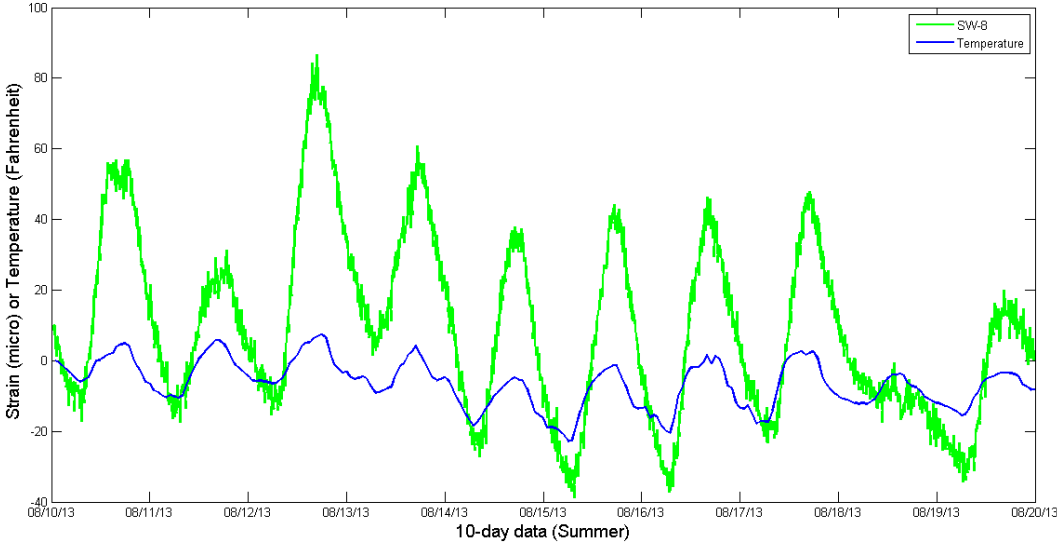


Figure 39 10 Day Time History of Strain in S_W8 and Relative Temperature

As can be seen from Figure 39, which was expected, is that fluctuations in temperature directly correlate with strains induced in the strain gauge. The higher the temperature the higher the strains induced. The next step is determining a relationship between temperature and this induced strain.

5.1.2 Linear Regression

To determine what type of regression techniques needed to be used, temperature was plotted as the independent variable with the corresponding strain's induced being the dependant variable for sensor S_W8. This can be seen in Figure 40.

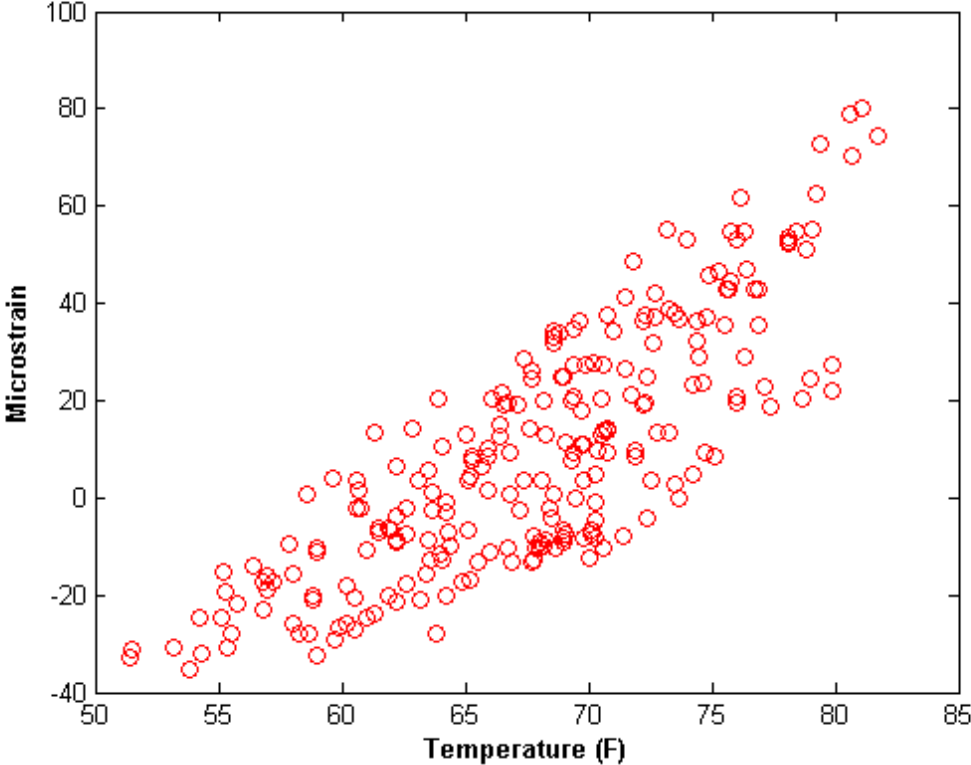


Figure 40 Temperature (Fahrenheit) versus Microstrain for Sensor S_W8

From an initial examination of the data, it could be believed that there is a linear relationship between temperature and microstrain. MATLAB code was then written in order to interpolate through the data to make it usable, followed by using the backslash command to fit a line through the data as well as calculating the coefficient

of determination (R^2) two ways to make sure it was correct. This code can be examined in Appendix A, section 1. The following figure, Figure 41 was generated from this code, along with an R^2 value of 0.69.

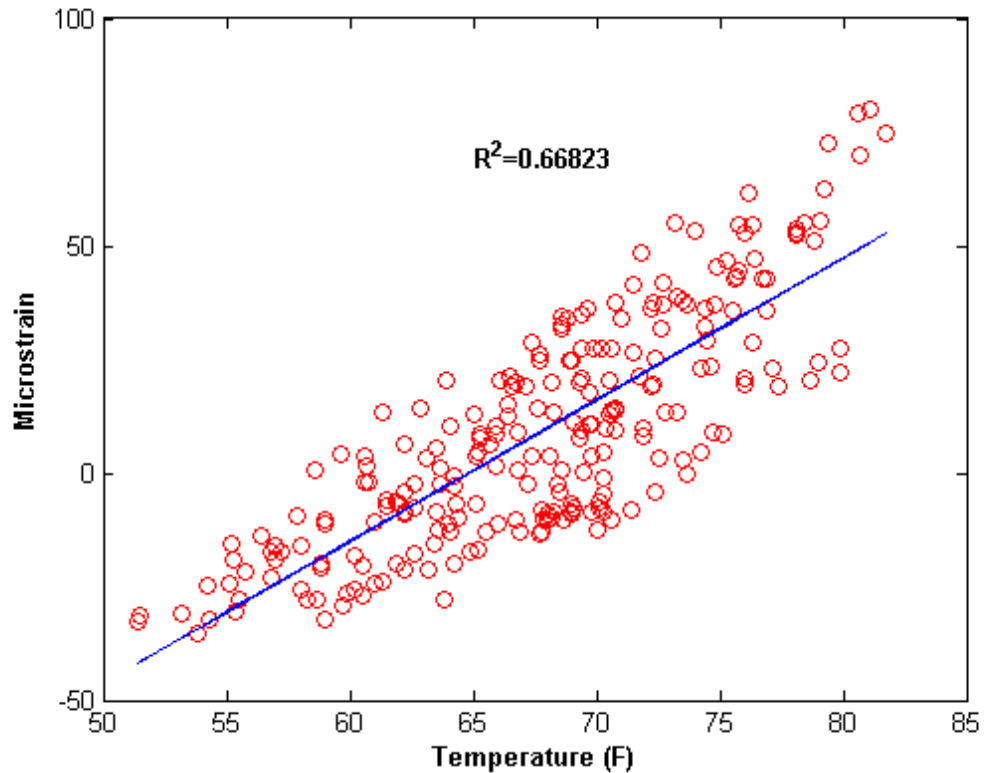


Figure 41 Linear Model for Microstrain as a Result of Temperature

This linear fit could be used to help predict the microstrain induced by temperature from the temperature recorded at the bridge for a specific time. The coefficients for the linear model give the following equation, equation 3.

$$(3) \mu\varepsilon = 3.12 * T - 202.14$$

The inputted value for Temperature (T) is in Fahrenheit and the outputted value is microstrain. Due to the R^2 value being only 0.67, which is a little far away from 1.0, it originally can be said that the linear model may not be the best predictor of strain.

5.1.3 Strain Curve Fitting

To investigate the strain response over this ten day period further, a sinusoidal model was developed from the strain data. In order to do so, the period was calculated for the ten day time series using a Fast Fourier Transform (FFT). The FFT determined that the period was 1 day. This value of one day would be expected due to the influence the sun has on the strains induced by temperature as the sun cycles from midnight to midnight of one day. Next, with this period, a regression was performed using the form of equation (4), outputting the coefficients of a, b and c. The equation used for the model is then represented by equation (5).

$$(4) \mu\varepsilon(t) = a \sin(2\pi t) + b \cos(2\pi t) + c$$

$$(5) \mu\varepsilon(t) = 4.8 \sin(2\pi t) + 25.47 \cos(2\pi t) + 9.28$$

This model compared to the actual temperature data from sensor S_W8 is located in Figure 42. The MATLAB code used to perform this modeling and plotting is located in Appendix A, section 2. Examining this model versus the actual response of S_W8 is interesting and shows some good observations about the data. The data's period matches very well to the predictive model. There are a few days in which the amplitudes match well too. These days may have been more moderate temperatures days that did not reach either extremes of very hot or very cold. The peak just before August 13th shows a hotter day compared to these nominal days, inducing larger strains. A day on the other side of the spectrum that was colder than normal was the

peak just before August 19th. If the data had a completely linear relationship there would not be such a large difference between the calculated sinusoidal model and the data on the more extreme temperature days. As a result of calculating this model, it further enforces the fact, along with $R^2 = 0.67$ for the linear model, that temperature and strain could possibly have a non linear relationship.

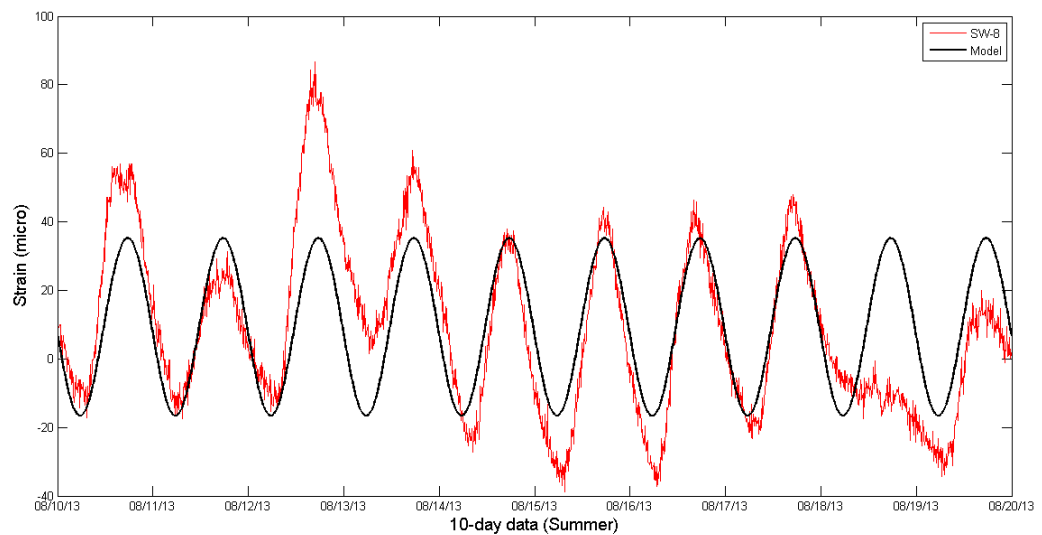


Figure 42 Strain Model (5) and S_W8 Over 10 Day Span

5.1.4 Non Linear Regression

Since the linear regression of the strain response only had a coefficient of correlation of 0.67, a nonlinear regression of the data was desired to see if it fit the data any better. The form used for this equation was a power equation with a constant added to it. The MATLAB function used to perform the regression of the power equation was `nlinfit`, which estimates the coefficients of a nonlinear regression function using least squares estimation. The code for this regression and plotting is

located in Appendix , section 3. After performing the fit, the equation of best fit is presented by equation (6) and can be seen in Figure 43.

$$(6) \mu\varepsilon = .183 * T^{1.569} - 127.64$$

Even though normally a R^2 value would not be calculated for a nonlinear regression, calculating it allows for a quick comparison to the linear model. The R^2 value for the power model was calculated to be 0.675.

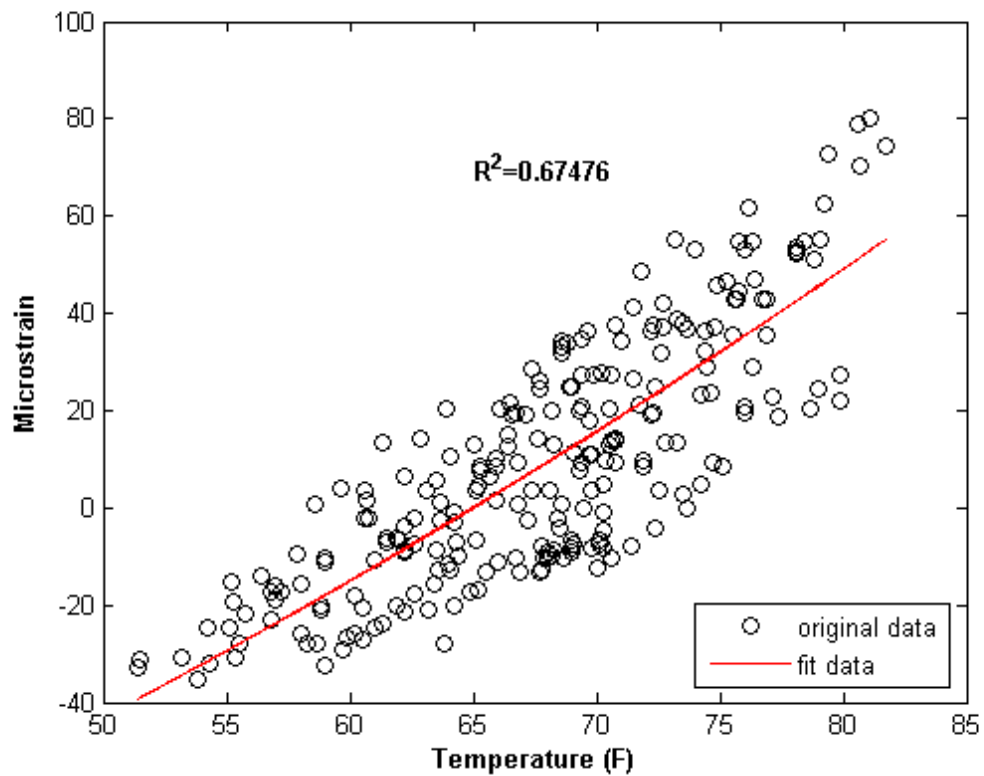


Figure 43 Power Model for Microstrain as a Result of Temperature

5.1.5 Discussion and Conclusions

Even though normally correlation coefficients would not be applied to nonlinear models, as a result of calculating the R^2 value for both models, it can be seen that they are almost statistically the same when it comes to accuracy. This then leads to the discussion of which model should be used. Within the data's range, from 50 to 85 degrees Fahrenheit, both the linear model and the power model can be used, resulting in accurate predictions. Outside of the data set used, at more extreme temperatures above 90 degrees and below 45 degrees, the power model only should be used, but may need to be adapted. At these extreme temperatures, it could be that the strains produced from temperature act more nonlinear. However, the best way to truly determine this would be to acquire a data set of many temperature measurements with their respective strains over an entire year. Then the power regression could be run again incorporating these many new points, allowing for a full picture of how the strain gauges react at all the different temperatures that the bridge experiences. This could possibly strengthen the nonlinearity of the data and make the power model much more accurate than a linear model.

Overall, with these models there is still a little bit of variance around the predicted value. This variance could hopefully be decreased in the power model by including the yearly data that would extend to much lower and higher values of temperature. This could possibly make the nonlinear model much stronger by adhering to the strain's nonlinear response at extreme values. For now however, the best model to predict strains based on temperature would be either the linear or power model within the data's range or the power model outside of the data's range.

All in all, by being able to predict the strain induced in a strain gauge by the temperature at the bridge, the temperature affects can be subtracted out of the strain

reading recorded at a time, allowing for only the affects of traffic to be seen. When temperature affects are negated and only traffic affects are seen, a trigger of a certain strain amount can be set for the entire year to tell the system when to record. When an induced strain is above this inputted limit, the system will turn on and record for a certain amount of time.

5.2 Permit Vehicles

There are numerous permit vehicles that travel over the Indian River Inlet Bridge. When one of these large load vehicles is going to travel over the bridge, the customer company needs to submit a permit for the truck. This report will detail the axle weights and spacing, total weight, fees, escorts, truck description, and the date the truck will travel over the IRIB. As a result of gaining access to these reports the SHM system was able to record the times when these trucks passed over. The following section details a few of the analysis that were done on this data.

5.2.1 Correlation of Strain to Truck Weight

As a result of the previous load tests, especially load test one, two equations were determined in order to relate peak strains from a sensor to truck weights. They are as follows in the form of equation (7) and (8):

$$(7) \frac{SW\ 22\ Peak\ Strain}{0.5055} = Vehicle\ Weight$$

$$(8) \frac{SE\ 22\ Peak\ Strain}{0.4772} = Vehicle\ Weight$$

These coefficients of 0.5055 and 0.4772 transform the peak strain data at SW_22 and SE_22 respectively into truck weights. Both of the numbers were obtained from load tests when the known weight of a single truck recorded a strain of

roughly half the truck weight. The coefficients vary based on which side of bridge under investigation due to the stiffer eastern edge girder as well as the pedestrian walkway. These numbers were attained from when the single trucks were in the slow lanes of the northbound and southbound directions individually.

Getting a conversion like this allows for an accurate estimation of how much a truck weighs based upon the strain induced in the bridge. This can help give a warning of when too heavy of a vehicle is going over the bridge based on a certain threshold that we set. Along with being able to see how heavy a truck is and the ability to zero the strain in the gauges with the temperature function, we can set a threshold limit for all times of the day that will trigger the system to turn on. For example the limit could be set at 60 kips and when the gauge experiences a strain corresponding to that weight or more, the dynamic collection rate is triggered to see the effects on the bridge.

5.2.2 Permit Peak Load Comparison

This idea of monitoring the bridge's strains and converting to vehicle weights can be applied to comparing permit loads reported to what strains are actually felt as the vehicle crosses. There will be 5 different permit loads that will be investigated. The loadings and resulting strains are located in table 7 and the wheel spacings are located in table 8 corresponding to Figure 44.

Table 7 Weight by Axle and Resulting Strains for Permit Vehicles

| Date | Gross Weight (kips) | Power Unit Axle Weights (kips) | | | | Trailer Axle Weights (kips) | | | Travel Direction | Peak SW_22 ($\mu\epsilon$) | Peak SE_22 ($\mu\epsilon$) |
|-----------|---------------------|--------------------------------|------|------|------|-----------------------------|------|------|------------------|------------------------------|------------------------------|
| | | 1 | 2 | 3 | 4 | 1 | 2 | 3 | | | |
| 8/13/2013 | 136 | 14 | 20 | 21 | 21 | 20 | 20 | 20 | SB | 50.6 | 28.4 |
| 8/15/2013 | 142 | 14 | 21 | 22 | 22 | 21 | 21 | 21 | NB | 50.7 | 48.7 |
| 9/5/2013 | 130 | 12 | 19.6 | 19.6 | 19.6 | 19.6 | 19.6 | 19.6 | NB | 31 | 47 |
| 9/6/2013 | 130 | 12 | 19.6 | 19.6 | 19.6 | 19.6 | 19.6 | 19.6 | SB | 56 | 27 |
| 9/16/2013 | 130 | 13 | 19.5 | 19.5 | 19.5 | 19.5 | 19.5 | 19.5 | SB | 58 | 36 |

Table 8 Wheel Spacing of Permit Vehicles

| Date | Wheel Spacings Center to Center (Feet) | | | | | |
|-----------|--|------|------|------|-----|-----|
| | A | B | C | D | E | F |
| 8/13/2013 | 15.5 | 4.5 | 4.5 | 35.5 | 4.5 | 4.5 |
| 8/15/2013 | 15.5 | 4.5 | 4.5 | 35.5 | 4.5 | 4.5 |
| 9/5/2013 | 11.33 | 4.67 | 4.67 | 36.5 | 4.5 | 4.5 |
| 9/6/2013 | 11.33 | 4.67 | 4.67 | 36.5 | 4.5 | 4.5 |
| 9/16/2013 | 13 | 4.75 | 4.75 | 34.5 | 4.5 | 4.5 |



Figure 44 Permit Vehicle Wheel Spacing Diagram

Interestingly we can then use these strains recorded from the permit loads to predict what we believe the actual load of the permit vehicle was. As a result of just taking a single edge girder's strain result at the controlling point, let's say the western, S_W22 and applying equation (7) we can get this approximate weight. Table 9 uses this technique showing the approximation of weight this gives us and compares it to the actual weight. This however is not the most accurate way to get the approximate weight of a permit vehicle due to the transverse load distribution of weight across the bridge. The resulting strains from the permit vehicles could be from a truck located in the fast lane or slow lane on either the northbound or southbound side of the bridge.

Table 9 Approximation of Permit Vehicle Weight Based on Equation (3)

| Date | Reported Gross Weight (kips) | Travel Direction | Peak SW_22 ($\mu\epsilon$) | Approximate Gross Weight From West (kips) | Percent Difference (%) |
|-----------|------------------------------|------------------|------------------------------|---|------------------------|
| | | | | | |
| 8/13/2013 | 136 | SB | 50.6 | 100.1 | 26.4 |
| 8/15/2013 | 142 | NB | 50.7 | 100.3 | 29.4 |
| 9/5/2013 | 130 | NB | 31 | 61.3 | 52.8 |
| 9/6/2013 | 130 | SB | 56 | 110.8 | 14.8 |
| 9/16/2013 | 130 | SB | 58 | 114.7 | 11.8 |

As can be observed from this table there is a wide range of percent differences when it comes to predicting approximate gross weights of the permit vehicles. The vehicles traveling southbound have the smallest percent differences due to their closer proximity to the strain gauge SW_22 leading to a more accurate prediction. The September 6th and 16th trucks have a low percent difference, which could possibly

result from the permit vehicle being in the western most lane. Since the adjustment factors used in equations (7) and (8) are from single trucks in the slow lane, these factors are adequate for permit vehicles traveling in the most western lane when using S_W22. The following assumptions of truck position are strictly based on percent difference of approximate to actual weight comparison. On August 13th, it can possibly be assumed that the larger percent difference comes from the truck being in the fast lane of the southbound side, creating larger variability. When the truck is traveling northbound, there is a much higher percent difference, especially for the truck on September 5th. It can be assumed that on September 5th the truck was in the northbound slow lane, while on August 15th the vehicle could have been in the northbound fast lane. These differences can also be attributed to the companies submitting their permits at a higher weight than what they actually expect their trucks to be so that they do not acquire fines for going over their reported limits. With the application of the previously computed transverse load distributions from a single truck moving transversely across the bridge, a more accurate prediction of the position of the trucks can be acquired. The actual positions of these trucks can be determined by the relationship of the strains in the eastern and western edge girders.

5.2.3 Transverse Load Distribution to Find Permit Vehicle Positioning

In order to find the probable lane location of each of the permit vehicles as they went over the bridge, the previously calculated transverse load distribution will be used. Figure 35 shows the percentages of loading from truck locations going from west to east, starting in the western shoulder and ending in the eastern shoulder. Taking this linear relationship, the transverse location of the vehicles can be recorded based upon the ratio of S_W22 to S_W22+S_E22. Even though Figure 35 uses data

from S_W8, this linear transverse distribution is seen across the entire bridge at many sensor locations which was confirmed in earlier sections of this paper. Located in table 10 is the probable location of each permit vehicle as it traveled over the bridge based upon the data conveyed in Figure 35. This is a more accurate way of determining where the vehicle was then the way in the previous section of looking at the percent difference between actual and approximate vehicle weights.

Table 10 Probable Locations of Permit Vehicles

| Date | Reported Gross Weight (kips) | Travel Direction | Peak SW_22 ($\mu\epsilon$) | Peak SE_22 ($\mu\epsilon$) | Percentage of Loading From West (%) | Probable Location, Figure 35 |
|-----------|------------------------------|------------------|------------------------------|------------------------------|-------------------------------------|------------------------------|
| 8/13/2013 | 136 | SB | 50.6 | 28.4 | 64.1 | SB Fast |
| 8/15/2013 | 142 | NB | 50.7 | 48.7 | 51 | NB Fast |
| 9/5/2013 | 130 | NB | 31 | 47 | 39.7 | NB Slow |
| 9/6/2013 | 130 | SB | 56 | 27 | 67.5 | SB Slow |
| 9/16/2013 | 130 | SB | 58 | 36 | 61.7 | SB Fast |

5.2.4 Two Truck Train Comparison and Weight Prediction

A better way of predicting the weight of a permit vehicle is comparing the permit vehicle to a two-truck train. A two truck train is very similar in the wheel spacing and layout as well as the weight. The first truck represents the power unit axles and the second truck represents the trailer unit axles with the larger space between the power unit and trailer unit axles being the space between the two trucks. Additionally, the sum of a two-truck trains weights is 128 kips which is comparable to the 5 reported weights of the permit vehicles investigated here. Located below is

Figure 45 which shows the strain time history data for the permit vehicle on September 6th, 2013. It can be seen that there are two spikes at the peak points of strain in Figure 45 which is representative of one spike being the power unit and the other being the trailer unit. This can also be seen in Figure 46 a typical result of a two-truck train going over an edge girder strain sensor. Figure 46 shows the response from Pass 2b of the April Load test. These two figures help exhibit the similarity between a two-train and a permit vehicle.

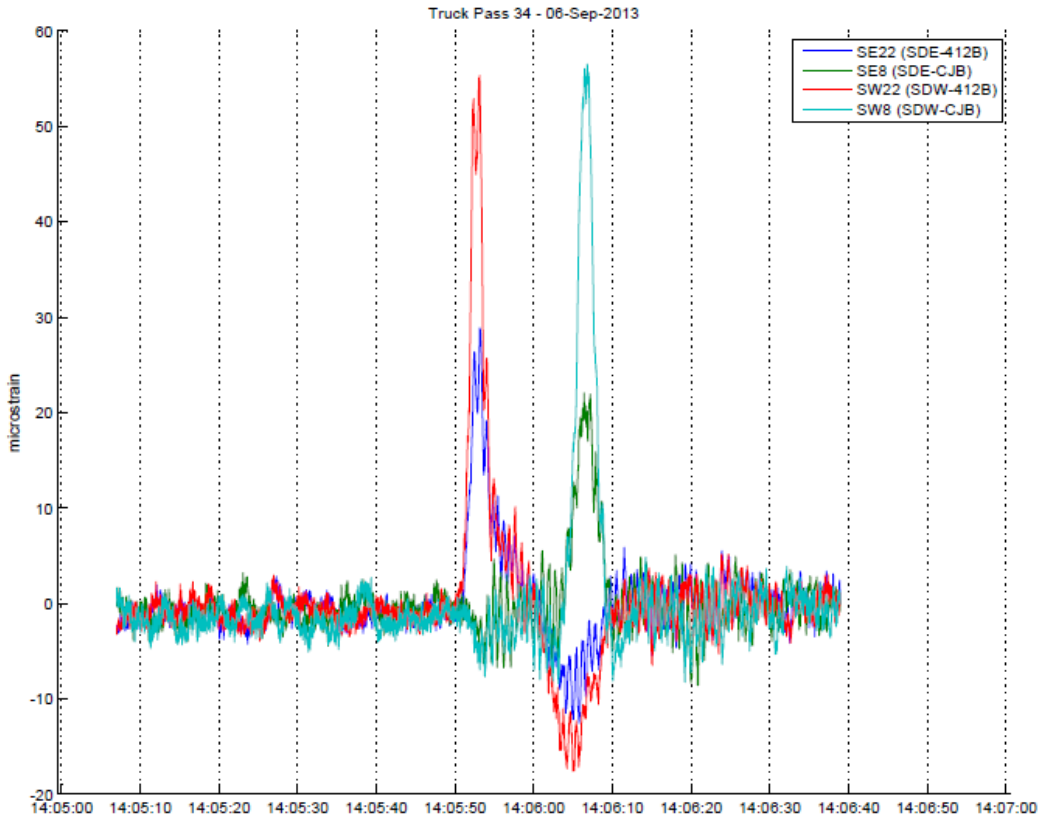


Figure 45 September 6th, 2013 Permit Vehicle Strain Time History

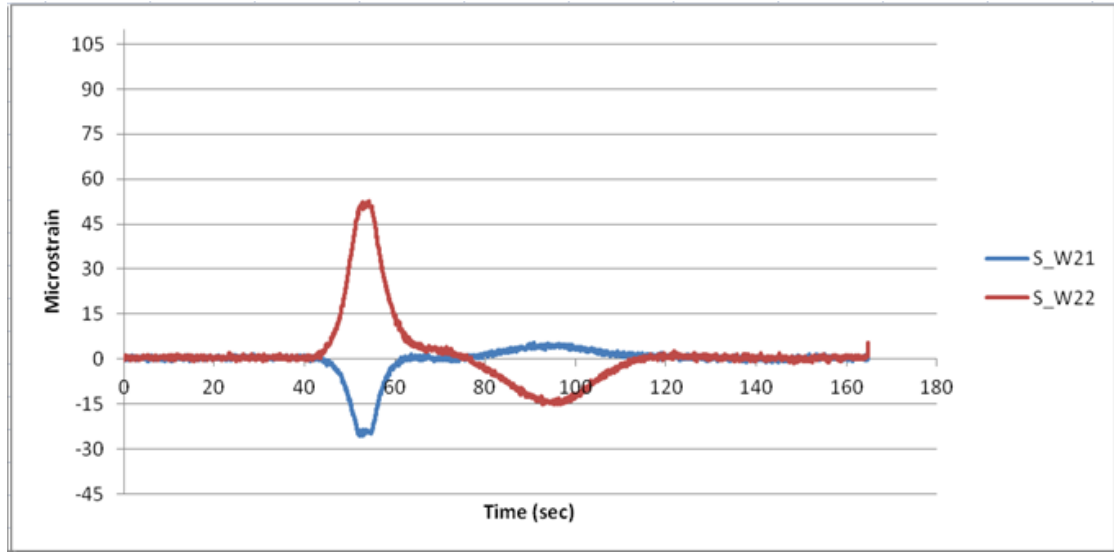


Figure 46 April Load Test, Pass 2b, Location SW_22

The next step is to use this comparison of the two truck train to the permit vehicle to determine the approximate weight of the permit vehicle. This can be done by using a ratio of the maximum recorded strains for both edge girders for the permit vehicle to the maximum recorded strains for the edge girders of the two truck train from the November Load Test. This ratio will then be multiplied by 128 kips (W_{LTT}), the weight of two of the test vehicles added together, to determine the approximate weight of the permit vehicle. Equation (9) shows this calculation well, with E standing for eastern edge girder, W standing for western edge girder, P standing for permit vehicle, and LTT standing for load for two trucks.

$$(9) \frac{\varepsilon_{WP} + \varepsilon_{EP}}{\varepsilon_{WLTT} + \varepsilon_{ELTT}} * W_{LTT}$$

For this all of these calculations the strain from the two-train load test in the western edge girder varied based upon the estimated position of the vehicle transversely across the bridge from the previous section. This estimate allows for the

most similar two-truck train pass's maximum aggregate of strains to be used, making the most accurate prediction of weight. September 6th uses Pass 2b, August 13th and September 16th use Pass 2c, August 15th uses Pass 2e, and September 5th uses Pass 2f. Table 11 shows the estimated weights of the trucks using this aforementioned technique.

This method of using two truck trains and their transverse positioning across the bridge is much more accurate than just using the factors in equations (7) and (8). The percent differences are much smaller and show a much closer estimate to the reported truck weights. Negative percent differences mean that the reported value submitted was lower than the actual truck weight. The trucks that correspond to these negative values could have possibly been subjected to fines for underreporting their truck weights. It is interesting to note that from our strain data collected, that the vehicles on September 16th and August 15th were both well over the truck weights that they reported. This could be due to other vehicles inducing a response in the examined strain gauges at the same time as the permit vehicle.

Table 11 Final Estimated Permit Vehicle Gross Weight

| Date | Reported Gross Weight (kips) | Probable Location | Permit Peak SW_2 2 (με) | Permit Peak SE_22 (με) | Load Test Peak SW_22 (με) | Load Test Peak SE_22 (με) | Estimated Permit Vehicle Gross Weight (kips) | Percent Difference Reported to Estimated (%) |
|-----------|------------------------------|-------------------|-------------------------|------------------------|---------------------------|---------------------------|--|--|
| | | | | | | | | |
| 8/13/2013 | 136 | SB Fast | 50.6 | 28.4 | 46 | 34.1 | 126.2 | 7.2 |
| 8/15/2013 | 142 | NB Fast | 50.7 | 48.7 | 39.2 | 42.3 | 156.1 | -9.9 |
| 9/5/2013 | 130 | NB Slow | 31 | 47 | 30 | 48.8 | 126.7 | 2.5 |
| 9/6/2013 | 130 | SB Slow | 56 | 27 | 52.6 | 26.8 | 133.8 | -2.9 |
| 9/16/2013 | 130 | SB Fast | 58 | 36 | 46 | 34.1 | 150.2 | -15.5 |

Chapter 6

FUTURE APPLICATIONS

6.1 Standard Test and Procedure Implementation

The load tests that are detailed in this paper were the first two to ever be conducted on the bridge, occurring at a six month interval from one another. There has been a third load test since then after another six months passed. After this third test, the bridge entered a cycle in which every two years the bridge will be load tested by a standard test that will be created. The goal is to have these tests be concise and give us the most useful data possible in the time conducting the test.

The standard test procedure has not yet been confirmed in any way yet but there are certain formations that I believe each test needs to include. These in my opinion are Passes 1a to 1f, 6a, 4f, and 4g. Pass 1a to 1f are one truck passes across the bridge from shoulder to shoulder. These are beneficial passes because they give a response of one heavily loaded truck, can confirm that the transverse load distribution across the bridge has remained the same, and will require that every part of the bridge has been loaded during the test. Pass 6a is necessary because it is the most extreme loading condition possible for the bridge and also can be used with the superposition of the one truck passes. Lastly, Passes 4f and 4g need to be used in order for the dynamic response of the bridge to be monitored.

With the use of these formations, with 2 passes lasting around 15 minutes, the test would take around two hours and fifteen minutes. When focusing on only necessary formations the test time is decreased by around 2 hours. A decrease in time

is beneficial because it allows for less time dedicated for everyone involved as well as lowers the possibility of congestion on the bridge.

The goal is then to provide DeIDOT with a boilerplate report about the bridge test, how the bridge responded, and recommendations on how to proceed in the future. Having a constant eye on the bridge, which would result from these reports, would keep DeIDOT informed on if the bridge is in immediate need of inspection or replacement.

6.2 Parameters to Observe

I believe that the parameter that must be observed and monitored in the future is strain data. The work of this paper mostly focuses on strain data outputted from the bridge because it gives a good picture of the health and functionality of the bridge. All the data that has been collected so far has been nominal to what we would expect. When the bridge begins to deteriorate over time is when observing strains will be very beneficial for knowing the performance of a bridge. If large strains began to be observed in a certain location on the bridge someone would be assigned to go investigate the location. A larger strain in an area could result from damages such as the spalling of concrete, crashes on the bridge, large ships impacting the superstructure, and corrosion over time, just to name a few. Abnormal strain data will help alert DeIDOT to structural issues with the bridge.

6.3 Long Term Use

The systems long term use is to monitor the bridge over its life span and produce reports at a certain interval based on what has occurred during the said interval. The structural health monitoring system will be turned on during extreme

predicted events such as hurricanes, but will also record everyday traffic that meets a certain criteria. When the system reads a strain over a certain threshold it will turn on and record data that can be used in the report. Overall, the goal is to create an autonomous system that generates reports that can be viewed by DeIDOT bridge engineers to keep up to date on the performance of the bridge.

Chapter 7

CONCLUSION

The work included in this paper gives the baseline response of the Indian River Inlet Bridge. Through examining such topics as peak strains, transverse load distributions, fundamental frequency, distribution factors, and maximum loading conditions, the nominal response of the bridge has been determined. These responses have been determined to be repeatable from comparisons between the first load test and the second load test conducted on the bridge. Such comparisons can be made in the future to confirm the fact that the bridge is operating at full capacity. As a result of temperature analysis, the amount of strain in a strain gauge can be determined based on the temperature from the weather station nearest the bridge. This will allow for a strain trigger to be set that follows a function based on the temperature of that specific day. Permit vehicles gave a good picture of high loading conditions and gave the opportunity to determine how to predict loads on the bridge based on strain data. Overall, the Indian River Inlet Bridge's integrated structural health monitoring system gives a high quality picture of the "health" of the bridge and has many future applications in both monitoring and research.

REFERENCES

- Akyrlmaz, O., R.N. Celik, N. Apaydun, T. Ayan. (2004). *GPS Monitoring of the Fatih Sultan Mehmet Suspension Bridge by Using Assessment Methods of Neural Networks*. ISPRS.org, Retrieved from <http://www.isprs.org/proceedings/xxxv/congress/comm7/papers/138.pdf>.
- Balageas, Daniel, Claus-Peter Fritzen, and Alfredo Guemes (Eds.) (2006). *Structural Health Monitoring*. New Port Beach, CA: ISTE USA.
- CTL Group. (2011). *A Case Study: Structural Health Monitoring of the Huey P. Long Bridge* (NA). Retrieved from <http://www.ishmii.org/wp-content/uploads/2011/06/Huey-Long-Bridge-Case-Study-revised-2011.pdf>.
- Doornick, J.D., B.M. Phares, Zhi Zhou, Jinping Ou, T.W. Grover, Zihang Xu. (2005). *Fiber Bragg Grating Sensing for Structural Health Monitoring of Civil Structures*. Micron Optics. Retrieved from <http://www.micronoptics.com/uploads/library/documents/FBGSensingSHMCivil.pdf>.
- Enckell, M. (2007). *Structural Health Monitoring of Bridges in Sweden*. 3rd International Conference on SHMII. Retrieved from <http://195.186.87.211/Bibliography/PDF/C183.pdf>.
- Inaudi, Daniele, Ren Deblois, Alan Phipps, Kevin Western, Cathy French, Jon Sebasky (2009). *Structural Health Monitoring System for the New I-35W St Anthony Falls Bridge*. 4th International Conference on SHMII. Retrieved from <http://www.roctest-group.com/~rtgroup/sites/default/files/bibliography/pdf/c202.pdf>.
- Jiang, Jianjing, Xinzheng Lu, Jingjun Guo. (2002). Study for Real-Time Monitoring of Large Span Bridge Using GPS. *Progress in Safety Science and Technology*, Tai'an September, 308-312. Retrieved from <http://luxinzheng.net/publications/11.pdf>.
- Mufti, Aftab A. (2002). *Structural Health Monitoring of Innovative Canadian Civil Engineering Structures*. *Structural Health Monitoring*, 1, 89-103. Doi: 10.1177/147592170200100106.

- Schulz, Whitten L., Joel P. Conte, Eric Udd (2001). *Long Gage Fiber Optic Bragg Grating Strain Sensors to Monitor Civil Structures*. Blue Road Research. Retrieved from <http://www.dtic.mil/cgi-bin/GETTRDoc?AD=ADA450831>.
- Shenton, Harry W. (2011) *Structural Health Monitoring of the Indian River Inlet Bridge*. 5th International Conference on SHMII.
- Stuffle, Timothy (2006) *The Indian River Inlet Bridge: Changing from a Single Rib Tied Arch to a Cable-Stayed Design*. (Master's Thesis) Retrieved from University of Delaware Library (UMI Number: 1435846).
- SMARTEC. (2008). *Overview of 40 Bridge Structural Health Monitoring Projects (IBC 09-45)*, Retrieved from <http://www.rocest-group.com/-rtgroup/sites/default/files/bibliography/pdf/c197.pdf>.
- West, Julia C. (2005). *Structural Health Monitoring of a Signature Bridge* (Master's Thesis) Retrieved from University of Delaware Library (Ascension Order No. TA 999 2005 W518 2005).

Appendix A

MATLAB CODE

A.1 Linear Regression

```
load('summerdaydata2.txt'); %loads strain data
load('summerdaytime2.txt'); %loads times that go with this strain
data

%We will focus on sensor S_W8 because it had the most sinusoidal
curve-like
%fluctuations in strain over a provided ten day period in the summer.
A ten
%day period will be examined, not just a day, in order to give the
full
%effect of the temperature over time on strains. S_W8 is at the
center of
%the bridge and is well exposed to the elements.

%Strain Data
strdata=summerdaydata2; %data
strtime=summerdaytime2; %time

%Temperature Data with Strain Data
tempdata=load('tempforday2.txt');
temptime=load('temptimeforday2.txt');

newstrain=interp1(strtime,strdata(:,8),temptime); %Takes points from
the
%strain data and makes it match up to the 240 points at which
temperature
%time has been taken

%The first days reading is taken and then zeroed in the original
%temperature data, tempdata, making the temperatures relative to
that..

actualtempdata = tempdata + 74.2; %On August 10, 2013 at midnight the
temp
%was 74.2 degrees F, must be added to make the temperature not
relative
```

```

%The last point is a NaN for the strain data, so the following for
loops
%cut off the last point, making the vector 239 points long.

for k=1:length(actualtempdata)-1
    cleanactualtempdata(k,1) = actualtempdata(k,1);
end

for k=1:length(newstrain)-1
    cleannewstrain(k,1) = newstrain(k,1);
end

X = [ ones(size(cleanactualtempdata)) cleanactualtempdata];
%X is a matrix used for linear regression, column of ones, and x
%(actualtempdata)

StrCoeffs = X\cleannewstrain; %Using backlash to get coefficients by
%regression

Strcurve = StrCoeffs(1)+StrCoeffs(2)*cleanactualtempdata;
%placing the coefficients into a first degree polynomial

%Calculate Rsquared value to see how good this fit is.
%Linear rsquared calc
ymean = mean(cleannewstrain)*ones(size(cleanactualtempdata));
%Makes a vector all with mean as entry

for i = 1:length(cleanactualtempdata)
    total(i) = (cleannewstrain(i)-ymean(i)).^2; %gets total sum of
squares
    residual(i) = (cleannewstrain(i)-Strcurve(i)).^2; %gets residual
sum of
    %squares
end
sumtotal = sum(total); %sum total sum of squares for all points
sumresidual = sum(residual); %sum residual sum of squares for all
points
rsquared = 1-(sumresidual./sumtotal) %calculates rsquared

[B,BINT,R,RINT,STATS] = regress(cleannewstrain,X);
check = STATS(1) %checks the rsquared value that I have calculated
using

    %regress function

plot(cleanactualtempdata,cleannewstrain,'ro') %plots the original
%temperature data versus the resulting strain
hold on
plot(cleanactualtempdata,Strcurve)%plots actual temp data versus the

```

```

%strain curve created by the regression
hold on
%Plot Set up

xlabel('Temperature (F)', 'FontWeight', 'bold')
ylabel('Microstrain', 'FontWeight', 'bold')
text(65,70, ['R^2=' num2str(rsquared)], 'FontWeight', 'bold')

```

A.2 Strain Fitting

```

load('summerdaydata2.txt'); %loads strain data
load('summerdaytime2.txt'); %loads times that go with this strain
data

strdata=summerdaydata2;
strtime=summerdaytime2;
%Temperature Data with Strain Data
tempdata=load('tempforday2.txt');
temptime=load('temptimeforday2.txt');

%Find the period of the Strain data over the ten day period
Fs = 1/(strtime(2)-strtime(1)) %Calculates sampling rate in hertz
NOVERLAP = [];
NFFT = length(strtime);
WINDOW=[1000];%Get a lot of windows to get a lot of points

[Pxx,F] = pwelch(strdata(:,8),WINDOW,NOVERLAP,NFFT,Fs);%determine
spectral
%density of the response
figure(1)
plot(F,Pxx)%plot frequency vs. power
set(gca, 'xtick', [0:5])
hold on
axis([0 5 0 2000])

maxpower = max(Pxx) %determine the value of the maximum power
maxpowerlocation = find (Pxx==maxpower)%Gives indicy of frequency of
max
%power
Period = 1/F(maxpowerlocation)%from frequency we get the period
%Out put is almost exactly one, which may correspond to one day.

X = [ ones(size(strtime)) cos(2*pi/Period*strtime)
sin(2*pi/Period*strtime)];
%X is a matrix used for regressions, column of ones, cos, sine

StrCoeffs = X\strdata(:,8); %Using backlash to get coefficients by

```

```

%regression

Strcurve = StrCoeffs(1)+StrCoeffs(2)*cos(2*pi/Period*strtime) +...
          StrCoeffs(3)*sin(2*pi/Period*strtime);
%Sets up the equation with the coefficients
figure(2)
plot(strtime, strdata(:,8), 'r')%plot real strain data
datetick('x','mm/dd/yy','keeplimits','keepticks');
xlabel('10-day data (Summer)','FontSize',14);
ylabel('Strain (micro)','FontSize',14);
hold on
plot(strtime, Strcurve,'k')%plot calculated strain curve
legend('SW-8','Model','FontSize',14);

```

A.3 Nonlinear Fitting

```

x=cleanactualtempdata; %the data, independant variable
y=cleannewstrain; %dependant variable

fh=@(c,x) c(1).*x.^c(2)+c(3); %defines what the function form is
and
%sets it as a handle
% guess values for parameters, use linear model for guesses(b0)
b0=[3.12,1.0,-202.14];
plot(x,y,'ko') %plots the original data
xlabel('Temperature (F)','FontWeight','bold')
ylabel('Microstrain','FontWeight','bold')
hold on

beta=nlinfit(x,y,fh,b0);% determine best fit coefficients
% plot the fit

plot(x,fh(beta,x),'linewidth',1,'color',[1,0,0]);
hold on
legend('original data','fit data','location','Best') % the
result
beta(1)
beta(2)
beta(3)

set(gcf,'visible','on')

ymean = mean(cleannewstrain)*ones(size(cleanactualtempdata));
%Makes a vector all with mean as entry
yfit = beta(1).*x.^beta(2)+beta(3);

for i = 1:length(cleanactualtempdata)

```

```

        total(i) = (cleannewstrain(i)-ymean(i)).^2; %gets total sum of
squares
        residual(i) = (cleannewstrain(i)-yfit(i)).^2; %gets residual sum
of
        %squares
end
sumtotal = sum(total); %sum total sum of squares for all points
sumresidual = sum(residual); %sum residual sum of squares for all
points
rsquared = 1-(sumresidual./sumtotal)

xlabel('Temperature (F)', 'FontWeight', 'bold')
ylabel('Microstrain', 'FontWeight', 'bold')
text(65,70, ['R^2=' num2str(rsquared)], 'FontWeight', 'bold')

```